Leaf orientation and the spectral reflectance of field crops

Xiaochen Zou

Department of Geosciences and Geography
Faculty of Science
University of Helsinki
Finland

Academic dissertation

To be presented, with the permission of the Faculty of Science of the University of Helsinki, for public criticism in the auditorium room D101 of the Physicum building (Gustaf Hällströmin katu 2), on May 27th 2015, at 12 o'clock.

Helsinki 2015

Supervisors: **Dr. Petri Pellikka**
Professor
Department of Geosciences and Geography
University of Helsinki
Finland

Dr. Matti Mõttus
Academy Research Fellow, title of Docent
Department of Geosciences and Geography
University of Helsinki
Finland

Pre-examiners: **Dr. Sanna Kaasalainen**
Research Manager, title of Docent
Department of Navigation and Positioning
Finnish Geospatial Research Institute
Finland

Dr. Natascha Oppelt
Professor
Department of Geography
Kiel University
Germany

Opponent: **Dr. Jaan Praks**
Assistant Professor
Department of Radio Science and Engineering
Aalto University
Finland

Cover photo by Priit Tammeorg

Publisher:
Department of Geosciences and Geography
Faculty of Science
PO Box 64, FI-00014 University of Helsinki
Finland

ISSN-L 1798-7911
ISSN 1798-7911 (print)
ISBN 978-952-10-9475-0 (paperback)
ISBN 978-952-10-9476-7 (PDF)
http://ethesis.helsinki.fi

Unigrafia Oy
Helsinki 2015

To my family

ABSTRACT

Leaf angle distribution (LAD) is one of the most important parameters used to describe the structure of horizontally homogeneous vegetation canopies, such as field crops. LAD affects how incident photosynthetically active radiation is distributed on plant leaves, thus directly affecting plant productivity. However, the LAD of crops is difficult to quantify; usually it is assumed to be spherical.

The purpose of this dissertation is to develop leaf angle estimation methods and study their effect on leaf area index (LAI) and chlorophyll a and b content (Cab) measured from optical observation. The study area was located in Viikki agricultural experimental field, Helsinki, Finland. Six crop species, faba bean, narrow-leafed lupin, turnip rape, oat, barley and wheat, were included in this study. A digital camera was used to take photographs outside the plot to record crop LAD. LAI and Cab were determined for each plot. Airborne imaging spectroscopy data was acquired using an AISA Eagle II imaging spectrometer covering the spectral range in visible and near-infrared (400–1000 nm).

A recently developed method for the determination of leaf inclination angle was applied in field crops. This method was previously applied only to small and flat leaves of tree species. The error of LAI determination caused by the assumption of spherical LAD varied between 0 and 1.5 LAI units. The highest correlation between leaf mean tilt angle (MTA) and spectral reflectance was found at a wavelength of 748 nm. MTA was retrieved from imaging spectroscopy data using two algorithms. One method was to retrieve MTA from reflectance at 748 nm using a look-up table. The second method was to estimate MTA using the strong dependence of blue (479 nm) and red (663 nm) on MTA. The two approaches provide a new means to determine crop canopy structure from remote sensing data.

LAI and MTA effects on Cab sensitive vegetation indices were examined. Three indices (REIP, TCARI/OSAVI and CTR6) showed strong correlations with Cab and similar performance in model-simulated and empirical datasets. However, only two (TCARI/OSAVI and CTR6) were independent from LAI and MTA. These two indices were considered as robust proxies of crop leaf Cab.

Keywords: leaf angle; leaf area index; leaf chlorophyll; digital photograph; imaging spectroscopy; PROSAIL model; vegetation indices

ACKNOWLEDGEMENTS

First and foremost, I would like to deeply express my gratitude to my supervisors, Prof. Petri Pellikka and Dr. Matti Mõttus. I would like to thank Prof. Pellikka for giving me an opportunity to pursuing my PhD in Finland and supporting me in research and life throughout time. I especially remember the time he picked me up at airport and helped me to settle down when I arrived at Finland. My special appreciation and thanks go to my thesis supervisor Dr. Mõttus. He introduced me to the world of physical remote sensing, encouraged and helped me to overcome the difficult obstacles throughout my studies. His wise guidance and advice have been of great value for me.

I am grateful to my co-authors Tuure Takala, Dr. Rocío Hernández-Clemente, Dr. Jan Pisek especially to Dr. Priit Tammeorg, Clara Lizarazo Torres, Dr. Frederick L. Stoddard and Prof. Pirjo Mäkelä from Department of Agricultural Sciences at the University of Helsinki. Without their kind cooperation, this thesis could not exist.

I wish to thank the two pre-examiners of this thesis, Dr. Sanna Kaasalainen and Prof. Natascha Oppelt for taking time to carefully review my thesis and providing constructive suggestions.

My sincere thanks go to all members in Geoinformatics Research Group for providing me generous help when it was needed. Thanks for sharing their thoughts and valuable discussions. It is a great honour for me to work with these excellent scientists. I have learned so much from all of them.

I would like to express my thanks for the supporting in dealing with the matters related to my PhD administration in the Department of Geosciences and Geography.

I also would like to thank my friends in Finland and China for their support and care.

I appreciated the financial support given by the China Scholarship Council, the Centre of International Mobility (CIMO), and the Faculty of Science at the University of Helsinki. I would like to acknowledge the Chancellor's travel grants at the University of Helsinki for supporting my conference travel in Poland.

Finally, I would like to dedicate this thesis to my parents for their endless support and love from childhood to now.

LIST OF ORIGINAL ARTICLES

I. **Zou, X.,** Mõttus, M., Tammeorg, P., Torres, C.L., Takala, T., Pisek, J., Mäkelä, P., Stoddard, F.L., Pellikka, P., 2014**.** Photographic measurement of leaf angles in field crops. *Agricultural and Forest Meteorology*. 184, 137–146.

II. **Zou, X.,** Mõttus, M., 2015. Retrieving crop leaf tilt angle from imaging spectroscopy data. *Agricultural and Forest Meteorology*. 205, 73–82.

III. **Zou, X.,** Hernández-Clemente, R., Tammeorg, P., Torres, C.L., Stoddard, F.L., Mäkelä, P., Pellikka, P., Mõttus, M., 2015. Retrieval of leaf chlorophyll content in field crops using narrow-band indices: effects of leaf area index and leaf mean tilt angle. *International Journal of Remote Sensing* (Submitted).

AUTHOR'S CONTRIBUTION

I was responsible for formulating the research questions, analysing the results, and composing the introduction and background of the three papers. In paper (**I**): I took the crop leaf photographs and scanned the leaf samples in the field. I also took the leaf angle measurements from leaf photographs. I pre-processed the AISA imaging spectroscopy data, including imagery georectification, radiometric correction and atmospheric correction. I performed all of the calculations and statistical analysis, composed the literature review for MTA measurements and drafted the first version of the manuscript's methods and results sections. In paper (**II**): I took the soil spectrum measurement in the field. I established the look-up table and made the PROSAIL model inversion. I performed the calculations and analysis, and drafted the first version of the manuscript's introduction, results, methods and discussion sections. In paper (**III**): I performed the vegetation indices calculations and statistical analysis. I drafted the first version of the manuscript. I coordinated the field data collections (LAI and leaf chlorophyll) with specialists from Department of Agriculture at the University of Helsinki, and this field data was used in papers (**I**) and (**III**). The final version of the three manuscripts (**I**), (**II**) and (**III**) were revised and improved by Mõttus and commented on by all the co-authors. The English grammar and usage in paper (**I**) was corrected by Dr. Stoddard.

LIST OF ABBREVIATIONS AND CRONYMS

AISA	Airborne Imaging Spectroscopy Application
BRF	Bi-directional Reflectance Factor
Cab	leaf Chlorophyll a and b content
Car	leaf Carotenoid content
Cm	leaf dry matter content
Cbp	leaf brown pigment content
Cw	leaf equivalent water thickness
CR	Canopy Reflectance model
GO	Geometric Optical model
HDRF	Hemispherical-Directional Reflectance Factor
IS	Imaging Spectroscopy
LAD	Leaf Angle Distribution
LAI	Leaf Area Index
LRF	Linear Regression Function
LiDAR	Light Detection And Ranging
LUT	Look-up Table
MTA	Mean Tilt Angle
NIR	Near-Infrared Radiation
POLInSAR	Polarimetric Interferometric Synthetic Aperture Radar
PROSAIL	Coupled PROSPECT and SAIL models
PROSPECT	Leaf level radiative transfer model
RD	Relative Difference
RT	Radiative Transfer model
RRMSD	Relative Root Mean Square Difference
SAILH	Scattering by Arbitrarily Inclined Leaves Hot spot model
STD	Standard Deviation
VI	Vegetation Index

CONTENTS

1. INTRODUCTION

1.1 Optical observation of vegetation

Vegetation covers approximately 100 million km^2, approximately 66%, of the land surface on earth and is an important component of the biosphere. It is involved in various biogeochemical cycles, for example, those of water and energy (Bonan et al., 2003). Plant canopy structure characteristics affect most ecological and agronomic processes, such as radiation interception, photosynthesis and evapotranspiration. Canopy structure is also an indicator of vegetation water and nitrogen status (Casa and Jones, 2004). Accurate estimates of vegetation biochemical and biophysical characteristics are important for modelling the exchange of energy and matter between the land surface and atmosphere (Houborg et al., 2007).

Canopy structure is characterised by the location, orientation, size and shape of the vegetation elements (Ross, 1981). One of the most important characteristics of canopy structure is leaf area index (LAI), which is defined as the one-sided leaf area per unit ground area (Watson, 1947). It is a critical structure parameter for understanding the exchange of energy, carbon and water fluxes in terrestrial ecosystems (Norman et al, 1995; Chen et al., 1999; Myneni et al., 2002). LAI is the main input parameter for simulating radiation and transmission through a vegetation canopy and is also a key input variable in the ecosystem productivity model (Knyazikhin et al., 1998; Liu et al., 1997; Colombo et al., 2003).

The second important plant canopy structure characteristic is leaf angle distribution (LAD). LAD plays a crucial role in controlling light interception in the canopy (Hikosaka and Hirose, 1997; Utsugi, 1999; James and Bell, 2000) and has a strong impact on energy and mass balance in a soil-vegetation-atmosphere-transfer system (Thanisawanyangkura et al., 1997; Werner et al., 2001; Baldocchi et al., 2002; Falster and Westoby, 2003). For a simple horizontally relatively homogenous plant canopy, LAD and LAI are the only two structure parameters characterising radiation fluxes reflectance, transmittance and absorbance (Ross, 1981; Lang et al., 1985). A variety of mathematical description functions have been developed and used for simplifying LAD (de Wit, 1965; Goel and Strebel, 1984; Campbell, 1990; Weiss et al., 2004).

Plant pigments are integrally related to the physiological function of leaves and of tremendous significance in the biosphere (Sims and Gamon, 2002; Blackburn, 2007). Photosynthetic pigments include chlorophylls a and b and several carotenoids (Ustin et al., 2009). Chlorophyll enables light harvesting and determines photosynthetic capacity within leaf and plant productivity, and is also a good indicator of vegetation stress (Anderson, 1986; Carter, 1994; Peñuelas and Filella, 1998; Boegh et al. 2002). Foliar chlorophyll a and b content (Cab) is related to nitrogen content, thus monitoring Cab can provide information on fertilizer availability (Vina et al., 2004; Zarco-Tejada et al., 2004; Haboudane et al., 2008).

Traditional destructive *in situ* measurements of vegetation biochemical and biophysical variables are laborious and unfeasible for large-scale measurements. Destructive methods do not allow the measurement of structural variations over time for the whole canopy or a single leaf. By contrast, indirect optical methods provide a non-destructive way of measuring all these canopy characteristics. LAI can be

determined from the transmittance of light through the canopy (Weiss et al., 2004; Jokckheere et al., 2004). Leaf mean tilt angle (MTA) is determined through the inversion of the directional gap fraction below a canopy (Welles and Norman, 1991; Welles and Cohen, 1996). Portable chlorophyll meters (e.g., SPAD) provide a non-destructive method. They determine the chlorophyll optical absorbing features and are widely used in agricultural studies (Filella et al., 1995; Steele et al., 2008). These ground-based measurement methods are local and site-specific, and therefore not sufficient for ecosystem model applications in large areas.

To estimate vegetation variables consistently using multiple scales and multi-temporally, an appropriate option is remote sensing. During the past decades, remote sensing of vegetation biophysical and biochemical properties for various scales has gained importance. A variety of new approaches have been developed and validated. In the solar radiation domain (400−2500 nm), various algorithms and models have been developed for different sensors, ranging from multispectral instruments to imaging spectrometers, from low to high spatial resolution instruments (Soudani et al., 2006; Colombo et al., 2008; Berni et al., 2009; Guanter et al., 2014). In recent years, the emergence of Light Detection and Ranging (LiDAR) and Polarimetric Interferometric Synthetic Aperture Radar (POLInSAR) technologies has resulted in the development of numerous methodologies to estimate vegetation structure and biochemical parameters (Praks et al., 2007; Le Toan et al., 2011; Kaasalainen et al., 2014; Nevalainen et al., 2014). Moreover, the multi-sensorial approach, which utilises the combination of radar and lidar data with optical dataset has gained interest (Moghaddam et al., 2002; Hyde et al., 2007; Mcinerney et al., 2010). The rapid development and wide application of remote sensing of vegetation make it an interesting and promising research subject.

1.2 Field measurement of vegetation biophysical variables

1.2.1 Field measurement of LAI

The validation and assessment of LAI estimation from remote sensing data is critical for large-scale observations (Weiss et al., 2007). Field measurements of LAI can be classified into three categories: direct, semi-direct and indirect methods. Direct methods include the destructive method and leaf litter collection method. An allometric relationship is an example of a semi-direct method. The most commonly used are the indirect methods of LAI determination from optical transmittance measurements.

Direct methods are the most accurate and can provide a reference for semi-direct or indirect methods. However, direct methods are laborious and time-consuming. For the destructive method, leaf samples need to be harvested and dry weighed. Leaf specific leaf area is determined from a small sample and used to convert dry leaf mass to leaf area (Jonckheere et al., 2004). Litter needs to be collected in traps distributed below the canopy during vegetation leaf fall, but for some species, leaves are replaced during the growing seasons, which makes this method problematic (Jonckheere et al., 2004).

LAI can be calculated from the forest inventory (e.g., tree height and stem diameter) using a semi-direct allometry method. LAI is linked to these inventory data through destructive sampling. Allometric estimates of LAI are comparable to those of other LAI measurements (Gower et al., 1999; Majasalmi et al., 2013). However,

allometric method is site and species-specific, and related to local climate conditions (Le Dantec et al., 2000).

Optical measurement techniques can make the LAI measurement fast and non-destructive (Morisette et al., 2006). When compared to allometric methods, the approach provides more accurate estimates of LAI (Smith et al., 1991). The principle of the optical method is to measure direct or diffuse light transmittance through the plant canopy (Jonckheere et al., 2004; Weiss et al., 2004) and infer LAI through radiative transfer theory (Beer-Lamber law) (Anderson, 1971; Ross, 1981). LAI is calculated from the canopy gap fraction:

$$P(\theta) = \exp(-G(\theta, \mathrm{LAD})\mathrm{LAI}/\cos(\theta)),$$

where $P(\theta)$ is the gap fraction, $G(\theta, \mathrm{LAD})$ is the G-function, the mean projection of a foliage area unit in a plane perpendicular to direction θ. $G(\theta, \mathrm{LAD})$ is dependent on LAD. For this gap fraction-based method, two assumptions are made: the distribution of leaves is horizontally uniform in the canopy and leaf size is small compared with the canopy. In reality, foliage is clumped; the distribution of leaves is not homogeneously uniform (Chen and Black, 1992). Furthermore, due to non-green canopy elements (e.g., stems, branches and flowers) interacting with the light, the optical method does not yield the LAI but "plant area index" (Neumann et al., 1989).

Many optical instruments have been developed for estimates of LAI, including LAI-2000 (Li-Cor, Lincoln, Nebraska, USA), SunScan (Delta-T Devices Ltd, Cambridge, UK), AccuPAR (Decagon Devices, Pullman, USA), DEMON (CSIRO, Canberra, Australia), TRAC (3rd Wave, Ontario Canada) and Digital Hemispherical Photograph (DHP). The SunScan device is well suited to a low uniform canopy (e.g., cereal crops) and widely used (Lambert et al., 1999; Sone et al., 2009; López-Lozano et al., 2010).

1.2.2 Field measurement of LAD

The traditional direct method for LAD measurement is to use clinometers in contact with the leaf surface (Campbell and Norman, 1998), which is laborious and time consuming. Some specialised instruments have been developed, for example 3D digitisers of plant elements (Sinoquet et al., 1998), portable spectropolarimeters for canopy-polarised reflectance measurements (Shibayama, 2004) and portable scanning lidar systems (Hosoi et al., 2009). As a result of the high cost of the instruments, these approaches are not widely used. Similar to LAI measurement is indirect measurement of MTA, which is conducted through the inversion of the directional gap fraction of canopy covers (Welles and Norman, 1991; Welles and Cohen, 1996). For example, MTA can be estimated from the gap fraction measurement of LAI-2000 and DHP. Due to the canopy structural effects on light transmittance, transmittance measurements yield large uncertainties. As a restult of the lack of LAD measurements, LAD is usually assumed to be spherical. Recently, a photographic leaf angle measurement method has been developed and validated in broadleaf tree species (Ryu et al., 2010; Pisek et al., 2011, 2013). This approach provides a fast, low-cost and repeatable LAD estimation. The uncertainty of photographic MTA measurement is within 4˚. Usually, crop leaves are different from those of tree species. For cereal crop species, the leaves are long and curved and thus cannot be measured directly from the photographs.

1.3 Imaging spectroscopy

Imaging spectroscopy (IS), or hyperspectral remote sensing, is the acquisition of images in many (tens to hundreds) narrow (<10 nm) contiguous spectral bands thus providing continuous spectral information. Imaging spectroscopy over multi-spectral data is the ability to select the wavelengths best suited for the application, even when these were not known at the time of data acquisition. Some of the widely used sensors are available either for space-or airborne-platforms. These imaging spectroradiometers are operated for research or commercial purposes.

The development of imaging spectroradiometers provided the capability to quantitatively estimate plant biophysical and biochemical variables. Many studies have focused on the retrieval of vegetation leaf pigments from IS data. One of the most important pigments retrievable using IS is leaf chlorophyll content (Zarco-Tejada et al., 2005; Zhang et al., 2008; Malenovsky et al., 2013; Hunt et al., 2013). IS data on canopy structure parameters estimation has also been developed. Leaf area index, one of the most important canopy properties, has received the most attention (Haboudane et al., 2004; Meroni et al., 2004; Darvishzadeh et al., 2011; Heiskanen et al., 2013; Xie et al., 2014), whereas few studies have been performed for LAD.

Imaging spectroscopy data provides continuous narrow bands in the visible and infrared spectral region. In order to retrieve the relationship between IS data and plant traits, a variety of methods and analyses are applied on IS data. Generally, two approaches are widely used. The first approach is to combine the IS data assimilated with the radiative transfer model. LAI, Cab and other vegetation parameters could be estimated. (Botha et al., 2007; Houborg et al., 2009; Jacquemoud et al., 2009; Kokaly et al., 2009; Vohland et al., 2010; Banskota et al., 2014). The second widely used approach is to establish an empirical relationship between vegetation variables and vegetation indices calculated from IS data (Oppelt and Mauser, 2004; Haboudance et al., 2008; Gitelson, 2012; Zhu et al., 2012; Hernández-Clemente et al., 2012).

1.4 Canopy reflectance models

The confounding effects on canopy reflectance are from canopy structure elements and leaf biochemical properties. The interaction of radiation inside the canopy is a complex process (Goel and Strebel, 1983). Physically based canopy reflectance (CR) models (following the physical laws of nature) can explicitly quantify the connections between canopy properties and canopy reflectance (Bothaet al., 2007). Physically based CR models can be classified as radiative transfer (RT) models, geometric optical (GO) models and computer simulation models. One type of RT model, referred to as the turbid medium model, assumes the vegetation canopy is composed of homogenous vegetation layers and the canopy elements are randomly distributed and form a “turbid medium”. The canopy is assumed to be infinite in the horizontal direction (Verhoef, 1984; Verstaete et al., 1990; Liang and Strahler, 1993). This model type is widely used for modelling canopy reflectance for field crops. One of the famous models is the light Scattering Arbitrarily Inclination Leaves (SAIL) model (Verhoef, 1984), which extended the Suit (Suit, 1972) model with variations of leaf inclination angles.

Computer simulation models are used for accurately computing radiation within a complex canopy configuration and validation of simplified analytical models. One of the typical models is the Monte Carlo ray tracing method (Ross and Marshak, 1988; Goel et al., 1991), but due to the large input parameters required, this type of

model is difficult to invert (Goel, 1988). A simpler approach known to work well in field crops needs to be chosen, although a simulation model would have worked.

One CR model can be run in forward mode (structural inputs: output canopy reflectance). The Canopy Bidirectional Reflectance Factor (BRF) can be computed for a certain set of canopy parameter combinations. Running a model in forward mode helps to elucidate the canopy properties' influence on reflectance (Rautiaine et al., 2004; Feret et al., 2011). The CR model can be applied to retrieve canopy properties from the measured spectral reflectance. The CR model is inverted by interpolating the degree of agreement between the CR models' simulated and measured spectra. A number of inversion approaches have been developed for different existing canopy reflectance models, including the iterative optimisation method (Jacquemoud et al., 1995, 2000; Meroni et al., 2004; Houborg and Boegh, 2008), look-up table (LUT) approach (Knyazikhin et al., 1998; Weiss et al., 2000; Combal et al., 2002; Darvishzadeh et al., 2012) and Artificial Neural Network (ANN) method (Gong, 1999; Weiss and Baret, 1999; Fang et al., 2003; Walthall et al., 2004; Bacour et al., 2006; Schlerf and Atzberger, 2006). In the iterative optimization method, the search algorithm may become trapped at a local minimum before achieving the global optimal value. LUT and ANN methods rely on a large database of simulated spectral reflectance. For the ANN method, it is time-consuming to train the neutral network method. The LUT approach is simple for inverting a CR model. A LUT is built-in advance of model inversion. It avoids the search trapping a local minimum and time-consuming model training.

The model inversion method has ill-posed problems (Atzberger, 2004; Combal et al., 2002): different model input parameter combinations might generate similar spectral features (Weiss and Baret, 1999) and no unique solution can be found. Prior knowledge of the model inputs (e.g.,model input parameters range) can constrain the model variables and improve the inversion accuracy (Combal et al., 2002; Lavergne et al., 2007).

1.5 Vegetation indices

Vegetation indices (VIs) are comprised of reflectance at a few discrete spectral wavelengths. VIs are widely used for extracting vegetation characteristics from remote sensing data (Broge and Leblanc, 2001; Hatfield and Prueger, 2010; Nguy-Robertson et al., 2014). Most of the indices are in employed ratio or normalised format of reflectance at two or three wavebands to improve the sensitivity of reflectance to interesting properties and reduce the effects of other factors (Carter, 1994; Gitelson and Merzlyak., 1994, 1997; Maccioni et al., 2001). Indices could be calculated from derivative spectra (Datt, 1999; Vogelman et al., 1993) or calculated as a combination of other indices (Daughtry et al., 2000; Haboudane et al., 2002; Wu et al., 2008). Many indices have been developed in specific spectral ranges to increase VIs sensitivity. For example, red-edge wavelengths are acquired from many satellite sensors to estimate chlorophyll content (Gitelson et al., 2005; Gitelson et al., 2012). Visible and near-infrared wavelength indices have been found to be sensitive to both chlorophyll content and LAI (Gitelson et al., 2002; Baret et al., 2007).

The empirical relationship between VIs and vegetation properties provides a simple and efficient approach for the remote sensing of vegetation. However, this approach lacks generality. Canopy reflectance is affected by the complex interaction between internal and external factors (Baret, 1991), which make the empirical

relationship be site, time and species-specific, and thus one VI cannot be directly applied on another study site or vegetation type (Baret and Guyot, 1991; Colombo et al., 2003; Gobron et al., 1997).

1.6 Research problems and objectives

The general purpose of this dissertation is to study the spectral reflectance of LAD in a crop canopy and the measurement methods. New LAD determination methods were developed from digital camera and airborne imaging spectroscopy data. This dissertation is comprised of three research papers.

I. LAD is an extremely important canopy structure characteristic. However, current LAD measurement methods are laborious, time-consuming, unfeasible or expensive. Due to the lack of LAD measurements, LAD is usually assumed to be spherical. Recently, a LAD measurement method has been developed and validated for tree species. As the tree species leaves are different from crop leaves, this method could directly apply in field crops. This paper extended the feasible and low-cost photographic LAD method to field crops.

II. The *in situ* photographic method is confirmed for LAD measurement in field crops in I. Field LAD measurement is local and site-specific. Thus, it is not possible to apply this method in a large area. In this paper, two remotely sensed MTA algorithms were developed.

III. Vegetation indices are widely used for Cab estimation. A number of VIs has been developed, tested and reported in the literatures. The effects of canopy structure on canopy reflectance and Cab sensitive VIs are complex. In this paper, the MTA and LAI effects on the performance of Cab sensitive VIs were evaluated.

2 MATERIALS AND METHODS

2.1 Study area

The study site was located at Viikki Experimental Farm, Helsinki, Finland (60.224˚ N, 25.021˚ E) (Fig. 1). Helsinki is situated at the southern edge of Finland. The yearly average temperature for Helsinki is 6˚C, and in the warmest month, July, the average temperature is 18˚C. In July and August 2011, it was warm at the begging of the period but quite wet at the end, as well as in 2012.

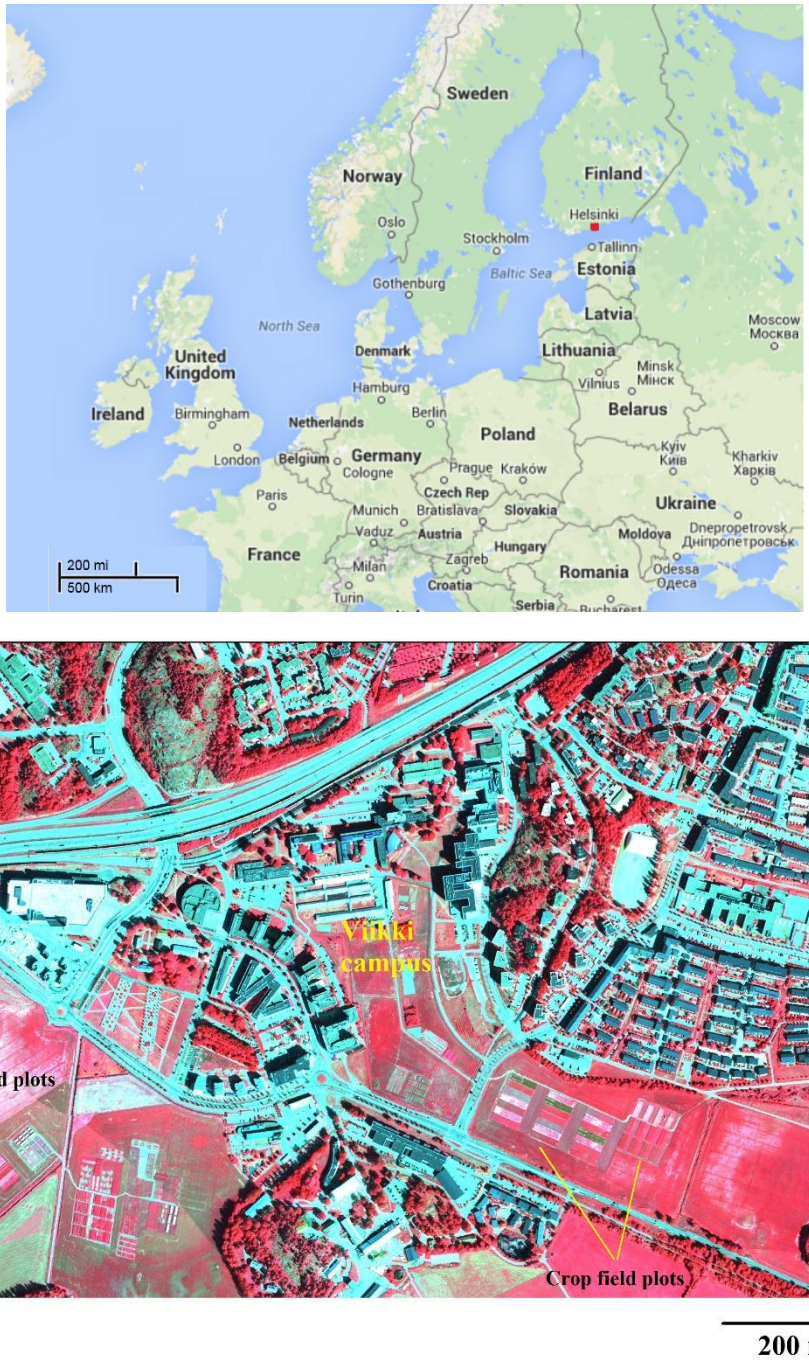

Fig. 1. a) Location of research area, b) AISA image of the test site (red: 814 nm, green: 691 nm, blue: 570 nm).

2.2 Test site

A total of 162 plots of six crop species (Fig. 2), faba bean (*Vicia faba* L. "Kontu"), narrow-leafed lupin (*Lupinus angustifolius* L. "Haags Blaue"), turnip rape (*Brassica rapa* L. ssp. *oleifera* (DC.) Metzg. "Apollo"), wheat (*Triticum aestivum* L.emend Thell. "Amaretto"), barley (*Hordeum vulgare* L. "Streif", "Chill" and "Fairytale") and oat (*Avenasativa* L. "Ivory" and "Mirella") were included in this study. The largest plot size was 50 m × 12 m and the smallest size was 10 m × 2 m. Different fertilizer treatments were applied for each species. The row space was 12.5 cm. During the series of field experiment periods, the crop canopy height was less than 1 m. The detailed description of plot size, number of plots, fertilizer application, seeding density and soil types are in I Table 1. The dataset used in this dissertation was taken from this study area.

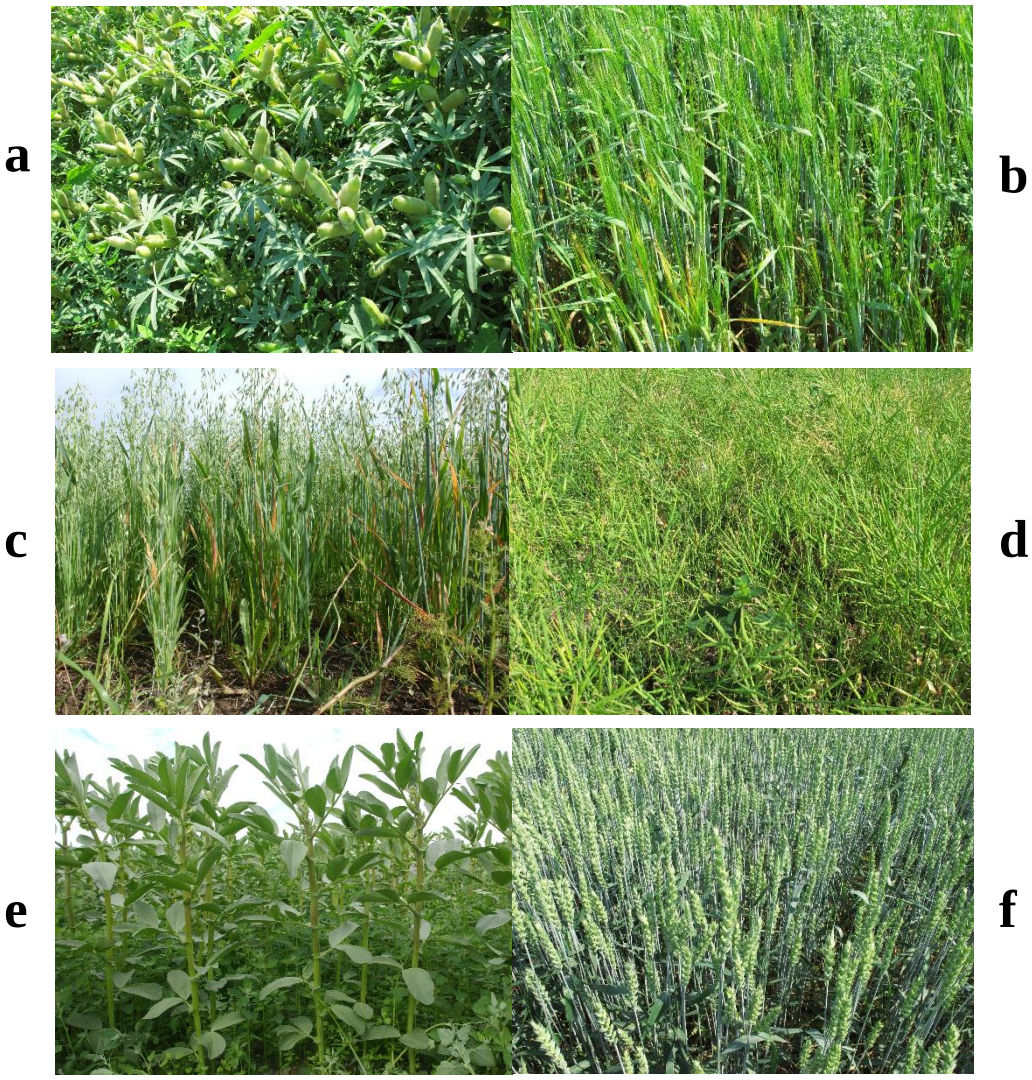

Fig. 2. Examples of the six crop species: a) narrow-leafed lupin, b) barley, c) oat, d) turnip rape, e) faba bean and f) wheat.

2.3 Field data

A brief description of the field measurement data used in this thesis is given in this section. The instruments used and the measurement times are summarized in Table 1.

Table 1. The instruments and measurement times for field measurement data.

Quantity	Instrument	Measurement time
LAD	Digital camera	6 July 2012
Leaf shape	Portable document scanner	3 August 2012
MTA	LAI-2000	5 − 6 July 2012
LAI	SunScan	20 − 21 July 2011
Cab	SPAD-502	19 – 22 July 2011
Soil spectrum	ASD	7 October 2011

2.3.1 Leaf angle measurement

Leaf inclination angle was measured using two approaches: a) a photographic method using a digital camera and b) an optical method using LAI-2000.

The crops were photographed using a Nikon D1X digital camera (Nikon Corporation, Tokyo, Japan) on 6 July 2012. The photographs were taken approximately 1m from the border of the plot, with the camera facing the crops. The camera was fixed on a tripod and levelled with a bubble level. The camera height was between 30 cm and 50 cm, depending on the crop height. The barley and oat plots were surrounded by grass. Before taking photographs, the grass was flattened so it would not obstruct the view. The plots for the other species were surrounded by areas of bare soil. Five to six photographs were taken for each species.

The LAI-2000 measurement was taken on 5 and 6 July 2012 for the plots for all six species (Fig. 3). Two or three plots were measured for each species. The measurements were taken 2 hours before sunset to avoid direct solar illumination from reaching the sensor. The measurement was taken along the plot edges. A 180˚ view restricting cap was used to minimise the effects from the observer and plot edge, and the detected solar radiation was entirely through the top surface of the canopy. The same sensor was used to measure below and above-canopy radiation. Depending on plot size, four to ten below-canopy measurements were taken and averaged for each plot. LAI-2000 measured radiation in five concentric rings and thus calculated canopy transmittance at five view zenith angles. MTA was calculated using an empirical polynomial relationship between the leaf angle and the slope of the G-function between 25˚ and 65˚ (Lang, 1986). The algorithm was implemented using FV2000 software provided by the instrument manufacturer.

2.3.2 Leaf shape measurement

Leaves of the three cereal crop species (wheat, barley and oat) were scanned using a USB-powered portable document scanner taken to the test site. For each species, 20 leaves were cut and scanned immediately. The images were stored on a PC in TIFF format (Fig. 4).

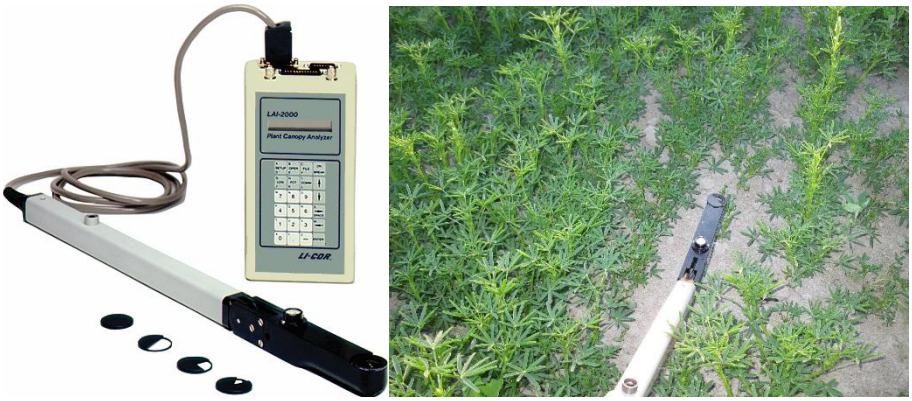

Fig. 3. LAI-2000 instrument and field measurements. Photographs by Annika Müller and Matti Mõttus.

Fig. 4. Scanned narrow and curved leaves (oat).

2.3.3 LAI measurement

LAI was measured weekly during the crop growing season in 2011. LAI was determined using a SunScan SS1 ceptometer rod (Fig. 5). Sixty-four miniature solar radiation sensors were mounted on the rod and each was aligned. The SunScan sensor was entered from the edge of the plot at approximately 45° to the crop row direction to minimise row effects. Simultaneously, a separate sunshine sensor type BF3 was recording outside the plot the direct and diffuse downwelling irradiance. LAI was computed from the radiance measurements, assuming exponential extinction of radiation inside the crop canopy. An ellipsoidal LAD model dependent on one parameter χ was used for the computations. As a default, spherical LAD was assumed, corresponding to $\chi = 1$. The computations were made using SunScan hardware. The full description of the algorithms is provided in the user manual (SunScan SS1 user manual version 2.0). The LAI of each plot was averaged from four to five readings. LAI data with the measurement date closest to the airborne flight campaign were used in this study; the used LAI measurements were taken within five days of airborne data acquisition.

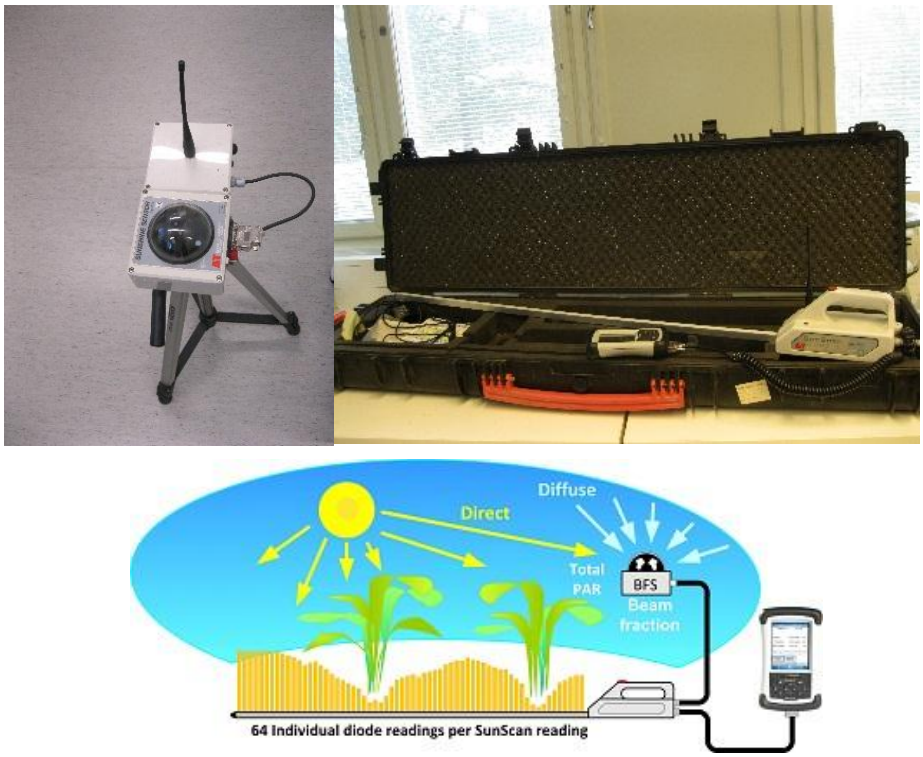

Fig. 5. The SunScan instrument: a BF3 sunshine sensor and the ceptometer rod in a carrying box. The schematic diagram provided by Delta-T Devices Ltd.

2.3.4 Leaf chlorophyll content measurement

Leaf chlorophyll a and b content (Cab) was determined using the SPAD-502 instrument (Minolta Corporation, Osaka, Japan) (Fig. 6). SPAD-502 is an optical device that measures leaf transmittance at wavelengths sensitive to chlorophyll and produces a unitless reading. The measurement dates of all the plots were within five days of airborne data acquisition. The 15 to 30 sampled leaves were randomly selected within each plot, depending on the plot size. The average SPAD value was used for the corresponding plot.

Fig. 6. SPAD-502 chlorophyll meter. Photograph by Clara Lizarazo Torres.

Fig. 7. Soil spectrum measurement. Photographs by Matti Mõttus

2.3.5 Soil spectrum measurement

The bare soil spectrum was measured using a handheld spectroradiometer manufactured by Analytical Spectral Devices (Boulder, Colorado, USA) (Fig. 7). The measurement was taken on a harvested area on 7 October 2011 between 11:30 and 12:30 local time (UTC+2:00). The solar zenith angle varied between 66.0˚ and 68.3˚. The spectral range was 400–1000 nm, which was the same as that for the airborne imaging spectroscopy data. Four soil samples were measured separately for four plots that were close to the place of LAD measurement. The averages of the four spectra were used as soil spectra for the whole study area. Before the measurement, the loose debris on sample surface was cleared away. A series of 5 to 15 radiance measurements was taken for each soil sample. A white Spectralon reference panel was measured before and after the soil sample measurements. The white reference panel measurements were interpolated to the time of each soil measurement. The soil Hemispherical-Directional Reflectance Factor (HDRF) was calculated from the radiance measurements of the soil and Spectralon.

The measured soil HDRF was transformed using a soil reflectance model. This model was developed by Walthal et al. (1985) and modified by Nilson and Kuusk (1989) to match the illumination condition during the airborne data measurement (solar zenith was 49.4˚). Based on the light reciprocity relationship, the measured soil HDRF was transformed to HDRF at the condition that the solar zenith was 49.4˚. The diffuse sky radiation was ignored in the transformation. After transformation, the soil HDRF increased by approximately 25%.

2.4 Imaging spectroscopy data

Airborne imaging spectroscopy data was acquired on 25 July 2011 using an AISA Eagle II imaging spectrometer (Specim Ltd., Oulu, Finland) (Fig. 8). The instrument had 1024 channels, of which 512 were used and binned into 64 channels covering the spectral range from 400 nm to 1000 nm. The spectral resolution was 9 nm to 10 nm. The flight direction was perpendicular to the solar illumination direction. The flight height was approximately 600 m. The ground spatial resolution was 0.4 m. The measurement was carried out between 9:36 and 10:00 local time. During the airborne measurement, the average solar zenith was 49.4˚. The imagery was radiometrically calibrated using the CaliGeo software package (Specim Ltd., Oulu, Finland) and georectified using Parge (ReSe Applications Schlapfer, Wil, Switzerland) via ground

control points and navigation records. Atmospheric correction was performed and radiance data was converted into reflectance using ATCOR-4 (ReSe Applications Schlapfer, Wil, Switzerland). The water vapour estimate used in the atmospheric correction was calculated from an AISA spectral measurement at water vapour windows (850–890 nm) and absorption (940 nm) wavelengths. The detailed description of the water vapor calculation algorithm was provided by Schläpfer et al. (1998). Aerosol optical thickness data from sun photometer observations approximately 4 km from the study area provided a visibility estimate of 47 km. Finally, spectra of each plot were extracted visually using ENVI software. Representative plot spectra for each species, with Cab and LAI values closest to the species mean, are provided in III Fig. 3.

Fig. 8. AISA flight campaign in 2011: aircraft, sensor and sample data.

2.5 Canopy reflectance modelling

2.5.1 PROSAIL model

The PROSAIL canopy reflectance model consists of the coupled PROSPECT-5 leaf level radiative transfer model and SAILH canopy level reflectance model (Verhoef, 1984; Kuusk, 1991). PROSPECT-5 uses six input parameters: leaf chlorophyll a and b content (Cab), leaf carotenoid content (Car), leaf dry matter content (Cm), leaf equivalent water thickness (Cw), leaf brown pigment content (Cbp) and leaf structure parameter *N*. The PROSPECT-5-simulated leaf bidirectional reflectance and transmittance were input into the SAILH model. The additional parameters used as inputs for the SAILH model were LAI, MTA, hot spot size parameter, soil reflectance, solar zenith angle, sensor view zenith and azimuth angle and fraction of incident diffuse sky radiation. The leaf level PROSPECT-5 model-simulated leaf reflectance and transmittance were used as inputs for the SAILH model, and then reflectance was simulated at canopy level. The PROSAIL model is a turbid medium RT model. It defines the vegetation canopy as a homogenous and infinite layer in the horizontal plane. The canopy elements are small compared with the canopy and act as absorbing and scattering particles. In this model, the one-parameter (MTA) ellipsoidal distribution model is used for characterising LAD. The assumptions of the PROSAIL model are very suitable for a field crop canopy.

2.5.2 Model input

The PROSAIL model input parameters were taken from the measurements. The values not available for the test site were taken from scientific literature. The leaf structural parameter *N* was fixed to 1.55, the average for the six crops provided in literature (Haboudane et al., 2004). Based on field measurements, Cab varied between 25 μg cm^{-2} and 100 μg cm^{-2}, LAI between 1 and 5, and MTA between 15˚ and 70˚. The Cw was in a reasonable range from 0.001 cm to 0.02 cm (leMaire et al., 2004; Darvishzadeh et al., 2008). The leaf dry matter content Cm of short-lived graminoids (wheat, oat and barley) was 0.004 g cm^{-2} (Vile et al., 2005). For the other three species, faba bean, turnip rape and narrow-leafed lupin, the Cm has been reported to vary from 0.003 g cm^{-2} to 0.008 g cm^{-2} (Mäkelä et al., 1997; Dennett and Ishag, 1998; Pinheiro et al., 2005). In the model simulations, Cm was fixed to 0.005 g cm^{-2}, the average value for the six species. Assuming that the crops had no withered leaves during the growing season, the brown pigment content was set to zero (Houborg et al., 2009). Car was linked to Cab based on the high reported correlation between the content of the two pigments (Feret et al., 2008). For the 17 herbaceous species (22 samples) in the LOPEX93 database (Hosgood et al., 1994), the average ratio of Car:Cab was found to be 1:5. This ratio was used in the model simulation. The hot spot parameter was fixed to 0.01, the default value of the model. The sensor and solar geometric parameters were coincided with the measurement conditions. The ratio of the direct and diffuse irradiance was calculated from the 6S atmospheric radiative transfer model (Vermote et al., 1997). The water vapour parameter for the model was generated from AISA imagery and the aerosol optical depth was taken from the observations of the sun photometer. The soil reflectance spectrum was taken from field measurements.

2.5.3 Database of reflectance spectra

For the feasible model input parameters, parameter values were randomly generated within the input parameter range. In total, 100,000 model inputs parameter combinations were built. All parameter combinations were used as model input. By running the model for each parameter combination, 100,000 spectrum data were simulated with 1 nm resolution. Finally, the spectrum data were resampled to correspond to AISA bands (binning the neighbouring spectrum reflectance central wavelength). The resampled spectrum and corresponding input parameters were combined as a LUT database.

2.5.4 Simulating the reflectance spectra of test plots

For the 162 field measured plots, plot-wise spectra were simulated using the PROSAIL model with the measured LAI, MTA and Cab as inputs. PROSAIL-simulated plot-wise canopy reflectance was compared with AISA measured reflectance in visible (452 nm, 551 nm and 682 nm) wavelengths, red edge (729 nm) wavelength and NIR (786 nm and 852 nm) wavelengths.

2.6 Data processing

2.6.1 Determination of LAD from photographs

The leaf inclination angles in the crop photographs were determined using the ImageJ software package (http://rsb.info.nih.gov/ij/). From the images, 75–100 leaves were measured. For the three species with flat leaves (faba bean, narrow-leafed lupin and turnip rape), the leaf inclination angle could be measured directly from the photographs as described by Pisek et al. (2011). The leaves that were perpendicular to the viewing direction and visible as straight lines in the image were selected. The angle between the leaf surface normal and zenith was measured as the leaf inclination angle: the angle between the line in the image corresponding to the leaf and the vertical direction (Fig. 9). Assuming the leaf orientation was randomly distributed with the azimuth direction, the selected leaves could be representative of all leaves.

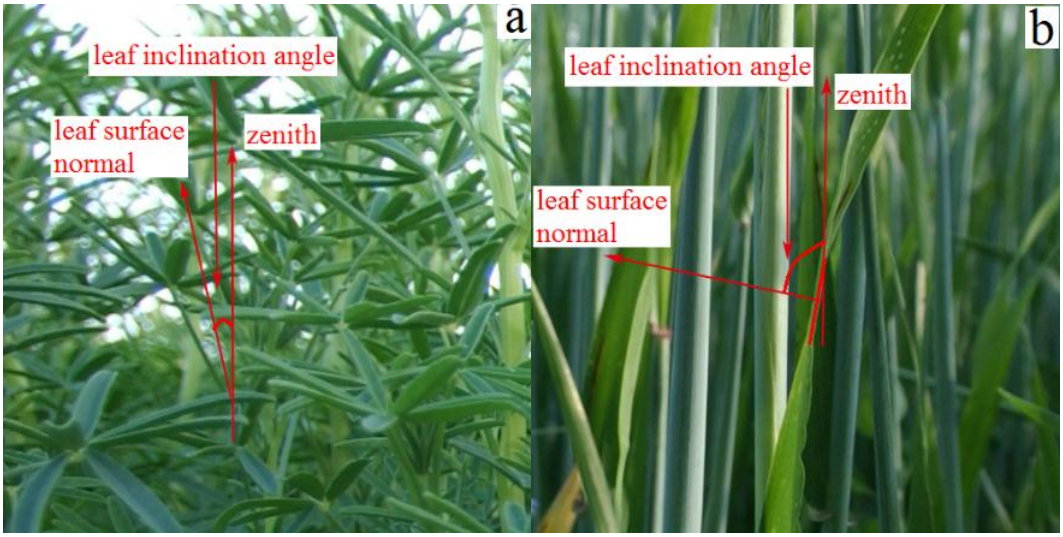

Fig. 9. Measurement of leaf inclination angle: (a) flat leaf (b) long and curved cereal leaf

For the three species with narrow and long leaves (wheat, barley and oat), the leaf inclination angle could not be measured directly from the photograph because there was no single leaf inclination angle for the whole leaf. The leaf inclination angle was measured segmentally after separating the leaf into measurable sections. The orientation of a section perpendicular to the viewing direction was measured using the same approach as for simple flat leaves. Simultaneously, the relative position of this section in the whole leaf was measured and recorded. This relative position on the whole leaf was converted into the relative leaf area via the leaf shape function. The relative area was used as the weight for each leaf segment.

2.6.2 Leaf shape function

The scanned leaves were divided into ten equal length sections in the leaf length direction. For each segment, the leaf width was measured and recorded. The leaf shape function was defined as the relative leaf width as a function of the relative distance in the leaf length direction (I Fig 2). The shape function was fitted using fourth order polynomial function. With the fitted leaf shape function, the relative area of any leaf section could be calculated using integration.

2.6.3 LAD: beta distribution

LAD was fitted using the two-parameter beta distribution function, which was demonstrated to be reasonable for fitting natural LAD (Wang et al., 2007). The distribution of the leaf inclination angle θ_L (or the zenith angle of the leaf normal) is quantified using the density function:

$$f(t) = \frac{1}{B(\mu,\nu)}(1-t)^{\mu-1}t^{\nu-1}, \quad (1)$$

where $t = 2\theta_L/\pi$, , and $B(\mu,\nu)$ is the beta function. The two parameters μ and ν are calculated as follows:

$$\mu = \left(1-\bar{t}\right)\left(\frac{\sigma_0^2}{\sigma_t^2}-1\right), \quad (2)$$

$$\nu = \bar{t}\left(\frac{\sigma_0^2}{\sigma_t^2}-1\right), \quad (3)$$

where $\bar{t}$ and σ_t^2 are the mean value and variance of t, respectively, and σ_0^2 is the maximum variance of t calculated as follows:

$$\sigma_0^2 = \bar{t}(1-\bar{t}). \quad (4)$$

For the leaf cereal species with curved leaves, the relative leaf area was used for each measured segment's angle as a weight. Thus, for these species, $\bar{t}$ and σ_t^2 were the weighted mean leaf angle and variance of t.

2.6.4 LAD: ellipsoidal distribution

Another important and commonly used LAD model is the ellipsoidal LAD model (Campbell, 1990). This distribution density function is expressed as

$$f(\theta_L) = \frac{2\chi^3 \sin\theta_L}{\Lambda(\cos^2\theta_L + \chi^2\sin^2\theta_L)}, \quad (5)$$

where θ_L is the leaf inclination angle and χ is a the ratio of the horizontal semi-axis length and the vertical semi-axis length of an ellipsoid. Λ is a parameter determined by χ. When $\chi = 1$, the distribution is spherical, $\Lambda = 2$:

$$\Lambda = \chi + \frac{\sin^{-1}\epsilon}{\epsilon},\ \epsilon = (1-\chi^2)^{1/2},\ (\chi \le 1), \quad (6)$$

$$\Lambda = \chi + \frac{\ln[(1+\epsilon)/(1-\epsilon)]}{2\epsilon\chi},\ \epsilon = (1-\chi^2)^{1/2},\ (\chi > 1). \quad (7)$$

LAD is described by one parameter χ; the relationship between χ and MTA is quantified as follows:

$$\chi = -3 + \left(\frac{\mathrm{MTA}}{553}\right)^{-0.6061}. \quad (8)$$

2.6.5 G-function

LAD is related to the extinction coefficient, which can be quantified using the Ross-Nilson G-function (Ross and Nilson, 1965). The G-function equals the projection of a unit leaf area on the plane perpendicular to beam direction and can be expressed as follows (Warren Wilson, 1967):

$$G(\theta) = \int_0^{\pi/2} A(\theta, \theta_L) f(\theta_L) \mathrm{d}\theta_L, \quad (9)$$

$$A(\theta, \theta_L) = \begin{cases} \cos\theta \cos\theta_L, & \text{if } |\cot\theta \cot\theta_L| > 1 \\ \cos\theta \cos\theta_L \left[1 + \frac{2}{\pi}(\tan\psi - \psi)\right], & \text{otherwise,} \end{cases} \quad (10)$$

where θ is the view zenith angle, θ_L is the leaf inclination angle, and

$$\psi = \cos^{-1}(\cot\theta \cot\theta_L). \quad (11)$$

We calculated $G(\theta)$ from the two-parameter beta distribution fitted to actual measurements as the function $f(\theta_L)$.

2.6.6 Correction of LAI estimates using species-specific MTA

Photographic species-specific MTA was used instead of the spherical LAD (χ = 1) assumption in the SunScan LAI calculation model. The species-specific LAD parameter χ was calculated from Eq.8 and utilised in the SunScan LAI calculation algorithm. The SunScan LAI algorithm was implemented using software. A more accurate LAI estimate was generated and compared with the original estimate.

2.6.7 Effect of LAD on spectral reflectance

The Pearson correlation coefficients between PROSAIL-simulated spectra and model input parameters (Cab, Cw, LAI and MTA) were calculated. To reduce the large unbalance within the dataset, the empirical dataset was grouped by LAI values (LAI: 1–2, 2–3, 3–4, 4–5 and 5–6) and species. Finally, the 162 plots were grouped into 16 groups by species and LAI intervals. The average reflectance was used for each group. The correlation coefficients between measured MTAs (photographic MTA and LAI-2000 MTA) and AISA-measured spectral reflectance were calculated for each AISA spectral band. Model-simulated canopy reflectance spectra were extracted in 1° MTA intervals starting at 15°, 30°, 40°, 50°, 60° and 69°. The spectral reflectance data were plotted in the red (663 nm)-blue (479 nm) plane.

2.6.8 MTA estimation algorithms

MTA was estimated from AISA spectral reflectance using two methods. One method was to invert the PROSAIL model through a LUT method from single reflectance at 748 nm. The Relative Root Mean Square Difference (RRMSD) between AISA

spectral reflectance and LUT spectral reflectance at 748 nm was calculated. For the LUT, the 100 MTA producing the lowest RRMSD were retrieved and the mean value was calculated.

The other method was based on a new rotated axes at 68.4˚ to the blue (479 nm) axis (slope=2.4). The "ratio axis" was defined perpendicular to the "brightness axis". There was a strong correlation between the MTA and ratio axis (μ) coordinate:

$$\text{MTA} = -6793\mu + 93, \quad (12)$$

which was generated from the model-simulated data used to convert plot-wise calculated μ into MTA. For each field plot, the ratio axis (μ) was calculated from AISA-measured spectra. Only species-specific MTA was available from photographic measurements. The spectroscopic data-estimated MTA was averaged for each species and compared with species-specific MTA.

2.6.9 Uncertainty of MTA estimation

For the PROSAIL model inversion method using LUT at red edge reflectance, the standard deviation was defined as *U*, which was calculated from 100 MTA values of the 100 canopy configurations producing the lowest RRMSD between LUT and AISA reflectance. For the brightness and ratio axes method, there is no unique relationship between MTA and μ, as each μ corresponded to an MTA range. Six narrow μ intervals of 0.00002 uniformly distributed from μ = 0.006 to 0.011 were created and the *U* of MTA was calculated for each interval. *U* was calculated for the narrow μ intervals. The six narrow μ intervals were converted into MTA using Eq.12. Hence, the relationship between *U* and the six MTAs was established. This relationship was linearly interpolated to calculate the *U* for each estimated species-specific MTA from AISA data. For some AISA-estimated MTA beyond the range of the six MTA values, a constant *U* corresponding to the extreme values of the six intervals was used.

To calculate the retrieval uncertainty of species-specific MTA *D* from imaging spectroscopy data, two uncertainties were considered. One uncertainty was from the retrieval algorithms *U*, the other was from the retrieved MTA variations within species, which were characterised by the standard deviation of the mean;

$$\text{STD}_{\text{mean}} = \frac{\text{STD}_{\text{species}}}{\sqrt{n}}, \quad (13)$$

where $\text{STD}_{\text{species}}$ is the species-specific standard deviation and *n* is the number of the plots for each species. The two uncertainties *U* and STD_{mean} were assumed to be independent of each other. Finally, the uncertainty *D* was calculated as follows:

$$D = \sqrt{STD_{mean}^2 + U^2}. \quad (14)$$

2.6.10 Vegetation indices

In totally, 58 published chlorophyll sensitive vegetation indices were calculated. Although model simulated data and imaging spectroscopy data were from the canopy level, some of the best performing leaf level indices were also included. The majority of indices belonged to two groups. The first group included simple ratio indices calculated as r_x/r_y, where r_x is the reflectance factor at wavelength *x* (15 indices). The second group were normalised difference indices $(r_x - r_y)/(r_x + r_y)$ or their modifications (23 indices). In addition to the two groups, 18 wavelength combination indices and two derivative spectra indices were tested in this study. The derivative

spectrum was calculated as the difference spectra between two neighbouring channels (Dawson and Curran, 1998)

$$D_{\lambda(i)} = (r_{\lambda(j+1)} - r_{\lambda(j)})/\Delta\lambda, \quad (15)$$

where $\lambda(i)$ is the midpoint between the central wavelengths of bands j and j+1, $\lambda(j)$ is the central wavelength of band j, r_λ is the reflectance at wavelength λ and $\Delta\lambda = \lambda(j+1) - \lambda(j)$.

All the vegetation indices were calculated using simulated and AISA data. The measured wavelength closest to that reported in the literature was used. The maximum difference in wavelength between the reported and used values was 5 nm.

2.6.11 Statistical analysis of the performance of indices

The coefficients of determination (R^2) between Cab and VIs were calculated for model-simulated and empirical data, and were referred to as the R^2-model and R^2-empirical, respectively. To determine the MTA and LAI effects on VIs, the R^2-model and R^2-empirical values were calculated at different LAI and MTA values. In model simulated data, two LAI intervals (LAI = 1−2 and LAI = 4−5) were selected, presenting low and high LAI values. For empirical data, the low LAI values were selected as LAI = 2−3 to increase the number of observations. In model simulated data, two MTA intervals (MTA = 15˚−20˚ and MTA = 60˚−65˚) were selected to represent horizontal and vertical MTA values. Due to the MTA distribution in the actual data, the MTA effects test could not be performed for empirical data.

Linear Regression Functions (LRF) were calculated between Cab and VIs in model-simulated data and empirical data, referred to as the LRF-model and LRF-empirical, respectively. To compare the difference between the LRF-model and LRF-empirical, the relative difference of the slope and intercept of the LRF-model and LRF-empirical was calculated for each index:

$$\mathrm{RD} = |X_{\mathrm{model}} - X_{\mathrm{empirical}}|/X_{\mathrm{model}}, \quad (16)$$

where X is the either the slope or intercept of the linear regression model and the subscript X denotes it is calculated from model-simulated or empirical data. The indices with high values for the R^2-model and R^2-empirical, and low values of RD for the slope and intercept, were assumed to be the best performing VIs.

3 RESULTS

3.1 LAD from the photographic method

The LAD for each of the six species was fitted from photographic leaf angle measurements (Fig. 10). Generally, disregarding measurement noise, the beta distribution fitted well with the measured LAD. Faba bean, narrow-leafed lupin and turnip rape showed more horizontal LAD (Fig. 10a-c) than wheat, barley and oat (Fig. 10d-f). Narrow-leafed lupin had the most horizontal leaves and oat had the most vertical leaves. For cereal crop species, the difference between the weighed and non-weighed LAD was evident. The weighted method made the maximum LAD move slightly towards to the more horizontal LAD values and the maximum effect was approximately 6˚ (I Table 3). One of the two beta distribution parameters υ varied between 1 and 3, and the other parameter μ was between 1 and 8. MTA was highly correlated with μ; the R^2 was 0.90. MTA had no correlation with υ (R^2 = 0.01).

The G-function for the six species could be separated clearly (Fig. 11). The G-function calculated from faba bean LAD was quite close to the G-function calculated from planophile LAD. The G-function of barley was inseparable with that of uniform LAD. The G-function of oat overlapped with that of spherical LAD. For cereal crop species, the weighting effect on the G-function was not ignorable. The non-weighted G-function of oat was that of electrophile LAD, but after weighting, the G-function became that of spherical LAD. The corresponding effects of weighting on the G-function can be seen in I Fig. 3b.

For five of the six species (excluding narrow-leafed lupin), the species-specific MTA measured using the photographic method and LAI-2000 were highly correlated (R^2 = 0.92) (Fig. 12). For these five species, the LAI-2000 determined species-specific MTA that were systematically larger than the MTA measured using the photographic method. When considering all six species, this correlation dropped to 0.29. The big variation in this correlation could be attributed to the large difference in narrow-leafed lupin MTA determined from the two methods. For the photographic method, the MTA of narrow-leafed lupin was 18˚ but the MTA reported by LAI-2000 was 62˚.

3.2 LAI corrections from species-specific MTA

The LAI corrected using species-specific MTA had a strong correlation (R^2=0.98) with the LAI calculated from SunScan using the spherical ellipsoidal LAD model. The slope and intercept of the linear regression function is provided in I Table 5 for all species. The slope was between 0.66 and 1.27, depending on the species and MTA measurement method. According to the photographic MTA determination, the LAD of the six species was more horizontal than the spherical LAD assumption. After the correction by photographic MTA, the estimated LAI changed 0-1.5 unit depending on the species.

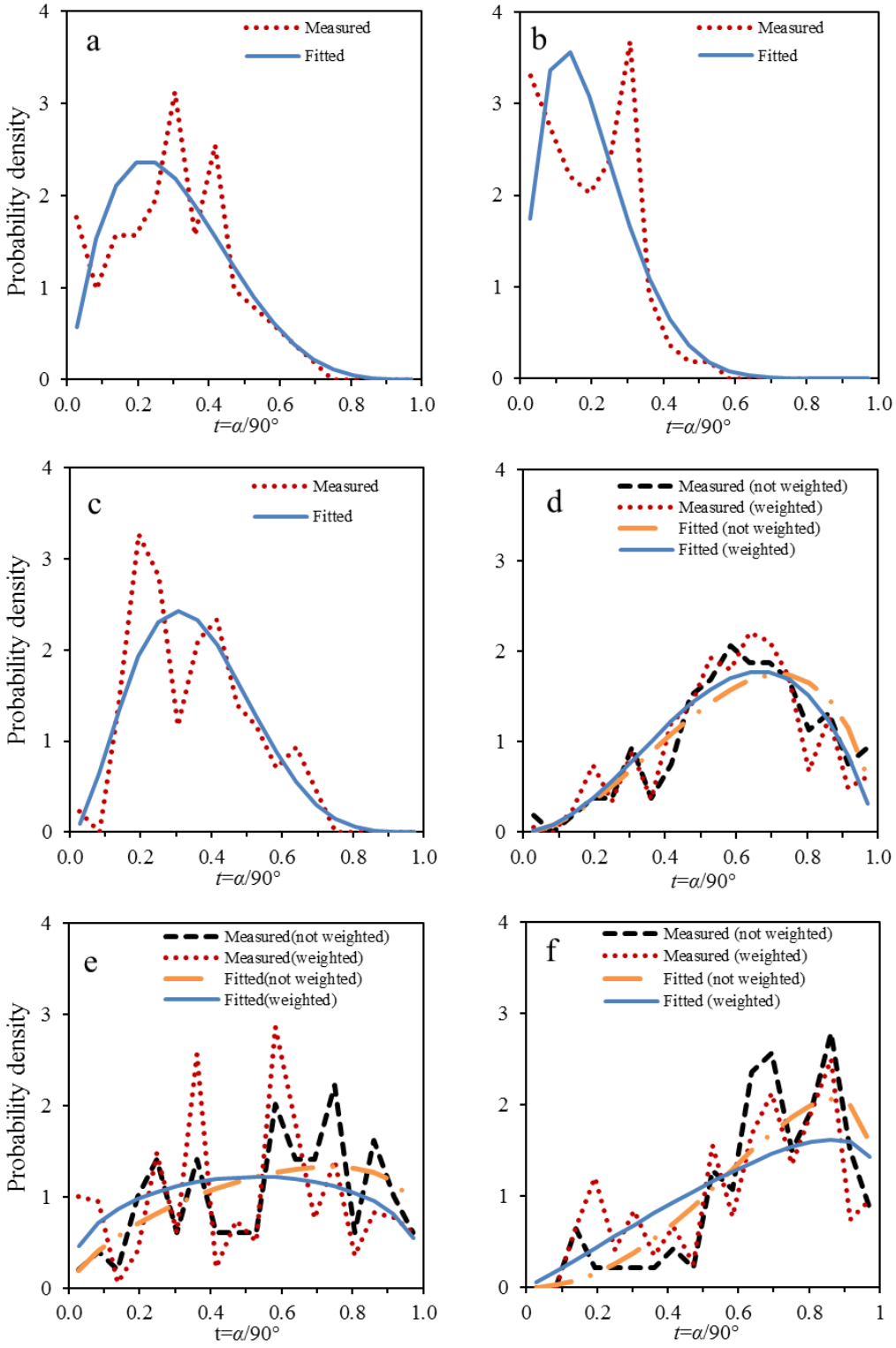

Fig. 10. Leaf distribution probability density measured using the photographic method and fitted by the beta distribution: (a) faba bean, (b) narrow-leafed lupin, (c) turnip rape, (d) wheat, (e) barley, and (f) oat. The leaf inclination angle α is measured from horizontal ($\alpha = 90^{\circ}$ indicates a vertical leaf)

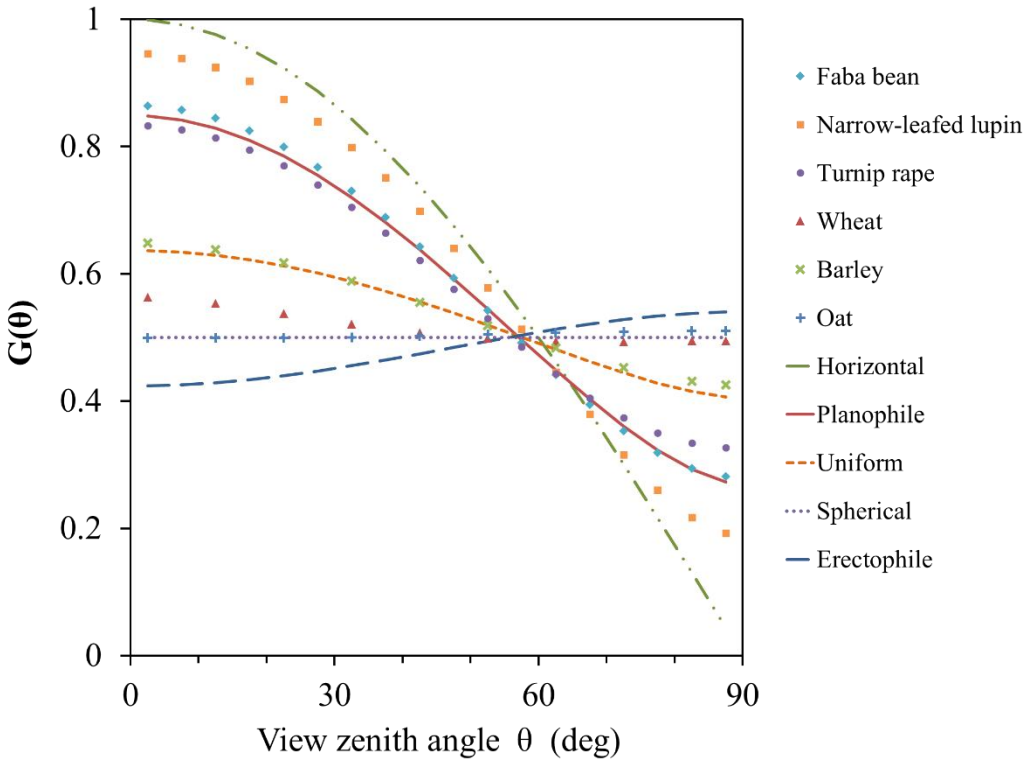

Fig. 11. The leaf projection function $G(\theta)$ calculated from beta distributions fitted to measured LADs as well as five theoretical LADs. For cereals (wheat, barley and oat), the G-functions were calculated using leaf-area-weighted beta distribution.

3.3 Crop spectra

Representative spectra for each species measured by the AISA spectroradiometer, with Cab and LAI values closest to the mean of each species, are plotted as representative crop spectra in Fig. 13. Comparing this with the AISA spectral measurement, model-simulated spectra were underestimated at the six wavelengths, especially at visible wavelengths (Fig. 14a). Reflectance simulated in NIR (Fig. 14b) was simulated more accurately than that at visible wavelengths.

In the model-simulated dataset, Cab was strongly correlated with BRF at the green and red edge, and had a sharp local trough at the 663 nm wavelength (Fig. 15b). MTA had a strong correlation with BRF at NIR especially at the far red edge. The highest correlation was found at the 748 nm wavelength with $R^2 = 0.78$ (II Fig. 6).

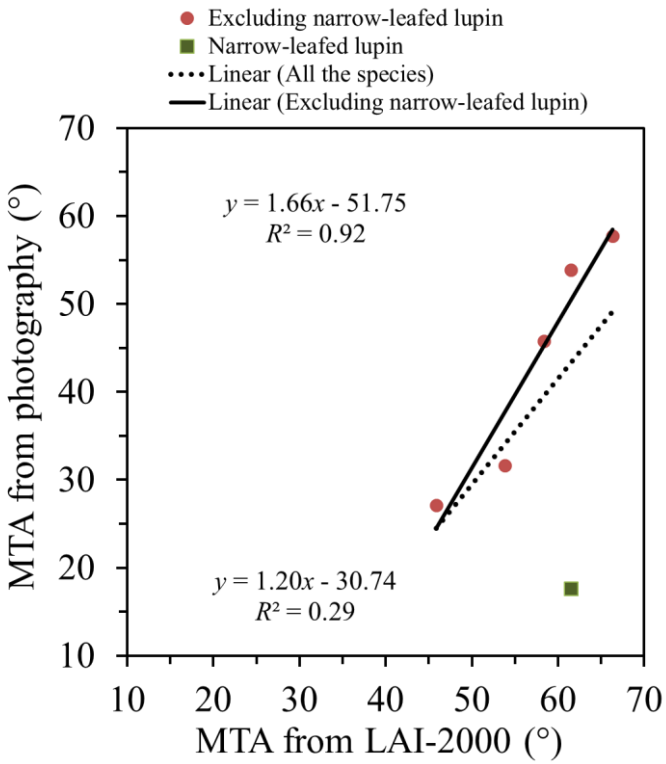

Fig. 12. The correlation between the species-specific mean tilt angles (MTA) determined using the photographic method and using the LAI-2000. A potential outlier, narrow-leafed lupin, is plotted with a filled square. Correlation coefficients and regression lines are given separately for all six species and for a subset excluding narrow-leafed lupin.

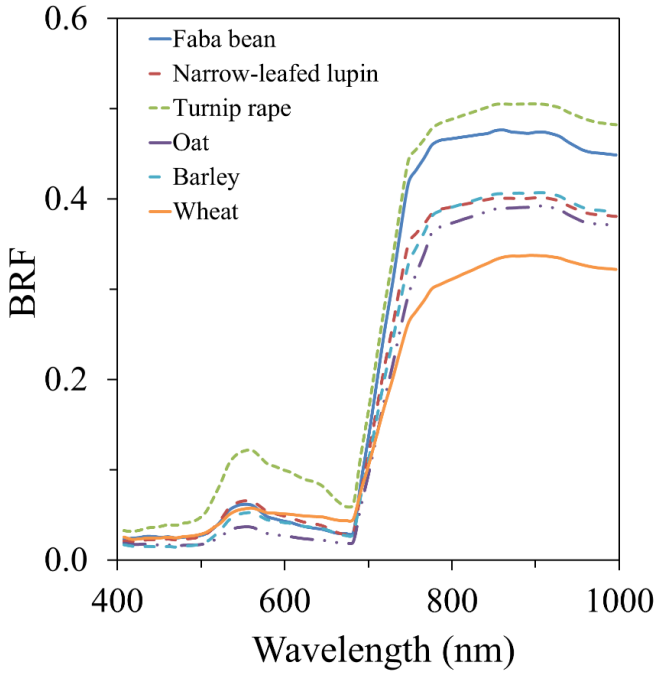

Fig. 13. Measured bidirectional reflectance factor (BRF) of the representative plot of each species.

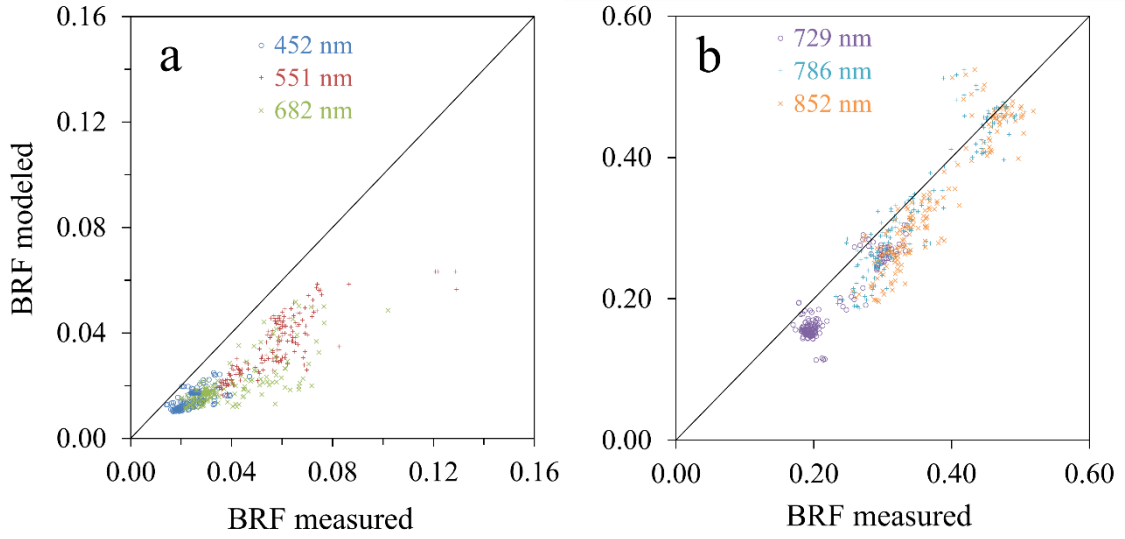

Fig. 14. AISA-measured and model-simulated reflectance factors at selected wavelengths: (a) visible light (452 nm, 551 nm and 682 nm), (b) the red edge and near-infrared (729 nm, 786 nm and 852 nm).

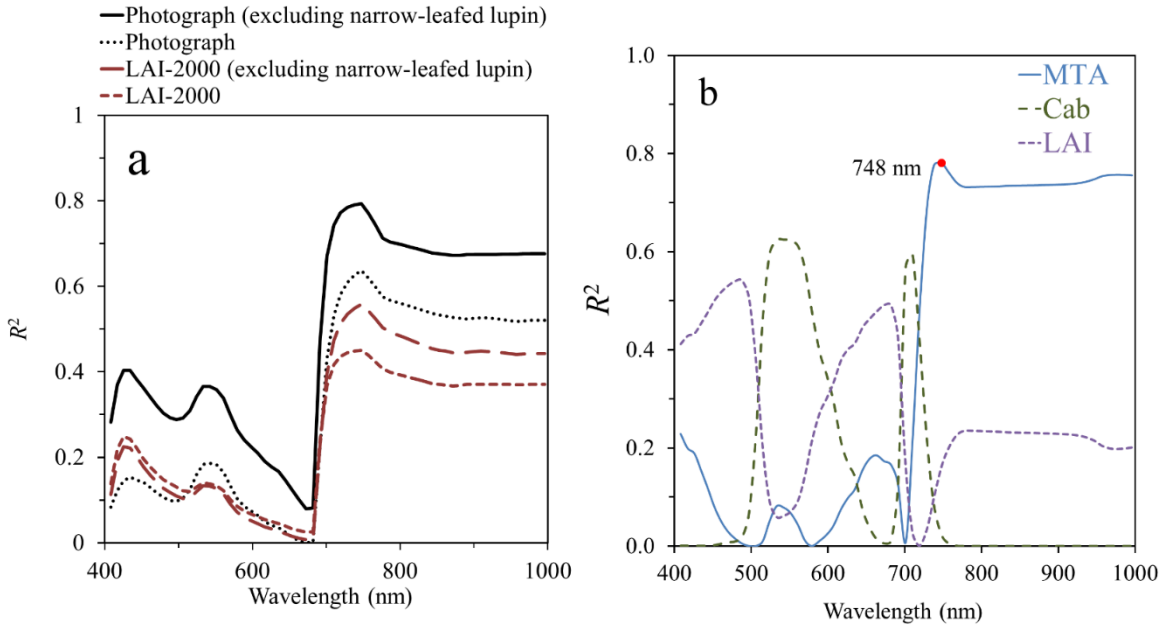

Fig. 15. a) The coefficient of determination (R^2) between spectral reflectance factor and MTA measured by both photographic method and LAI-2000. b) The R^2 between PROSAIL-simulated spectral reflectance and three variables: MTA, Cab and LAI.

This MTA-related spectral feature coincided with the empirical dataset (Fig. 15a and I Fig. 8). In the empirical dataset, the coefficient of determination between reflectance at 748 nm and MTA determined from photographs was 0.64 (I Fig. 8).

The reflectance at red (663 nm) and blue (479 nm) belonging to each MTA interval was highly correlated ($R^2 > 0.99$) (Fig. 16). The points were clustered and formed a straight line. These lines were separated clearly and nearly parallel with each other. The slopes of these linear regression functions varied between 2.1 and 2.9.

On the brightness and ratio axes, the coordinate brightness axis was mainly determined by LAI (II Fig. 3). The coordinate of the ratio axis was highly correlated with MTA (II Fig. 9). The six species were separated on the AISA spectra rotated brightness and ratio axes (II Fig. 5). Wheat occupied a range from 0.02 to 0.08 on the brightness axis. Turnip rape had the largest coordinates for both brightness (between 0.07 and 0.08) and ratio axes (between 0.012 and 0.014). Barley had the smallest value on the ratio axis (between 0.001 and 0.005). Although the ratio values for oat (between 0.007 and 0.008) overlapped with those for wheat on the ratio axis, they were separated on the brightness axis.

3.4 Determination of leaf angles from imaging spectroscopy data

Photographic species-specific MTA had a strong correlation with LUT-estimated MTA ($R^2 = 0.60$) (Fig. 17a). The RMSD was 11.4˚ between remotely-estimated and field-measured MTA. The MTAs of five of the six species (excluding narrow-leafed lupin) were underestimated using the red edge method compared with species-specific MTA (II Table 3). In Fig. 17b, the accuracy of MTAs estimated from the red-blue method was worse than that of the red edge method. The coefficient of determination between red-blue estimated MTA and field-measured MTA was 0.34, and the RMSD was 18.7˚. For different species, the red edge and red-blue methods had contrasting performances. For example, the MTA was well-estimated from the red edge for faba bean (RMSD = 3.2˚). The red-blue method yielded a MTA for this species with only average accuracy. The best-estimated MTA using the red-blue method was that of narrow-leafed lupin, but this species had the second-worse-estimated MTA from the red edge method.

In Fig. 18, for the red edge method, the standard deviation (STD) was a function of the retrieved MTA. The minimum STD was 4˚, corresponding to a retrieved MTA of approximately 20˚. The STD reached a maximum (approximately 11˚) when the retrieved MTA was approximately 40˚. With a further increase of retrieved MTA, the STD decreased to approximately 6˚. In Fig. 18, for the red-blue method, the STD varied between 1˚ and 5˚. When the retrieved MTA was between 15˚ and 50˚, the STD had a smooth variation between 1˚ and 2˚. When the retrieved MTA was over 50˚, the STD increased sharply to the maximum value.

3.5 Effect of canopy structure on Cab estimation

The 58 vegetation indices analysed in the study are ordered according to the R^2-model values in III Fig. 4. In model-simulated data, BGI showed the highest R^2-model value, followed by TCARI/OSAVI and Vogelmann (III Fig. 4). Approximately one-third of the VIs had an R^2-model value above 0.5. R^2-empirical was weakly correlated with the R^2-model. VIs that had R^2-empirical values above 0.6 (e.g., TACRI/OSAVI, REIP, MTCI, Datt3 and CTR6), had moderate R^2-model values (above 0.4), while others produced near-zero R^2-empirical values (Vogelmann, MCARI/OSAVI and

Datt4). Similarly, VIs that had high R^2-empirical values (e.g., NDVI1 and TCARI2/OSAVI2) only had moderate R^2-empirical values (approximately 0.4). The eight VIs that demonstrated above-average performance in both the empirical and model-simulated data were assumed as satisfactory indices (e.g., TCARI/OSAVI, REIP, MTCI, Datt3, CTR6, Datt5, NDRE, Datt2 and NDVI1).

In III Fig. 5, R^2 calculated for higher LAI intervals was larger than the R^2-model for lower LAI intervals for most of the VIs, except, for example, TCARI/OSAVI, CTR6, Datt4, DD and PSRI. In III Fig. 6, for most of the indices, R^2 produced from low MTA (greater horizontal leaf angle) was higher than R^2 calculated from high MTA (greater vertical leaf angle) interval data, while the R^2-model calculated from the full MTA range (15−70˚) was situated between the high and low

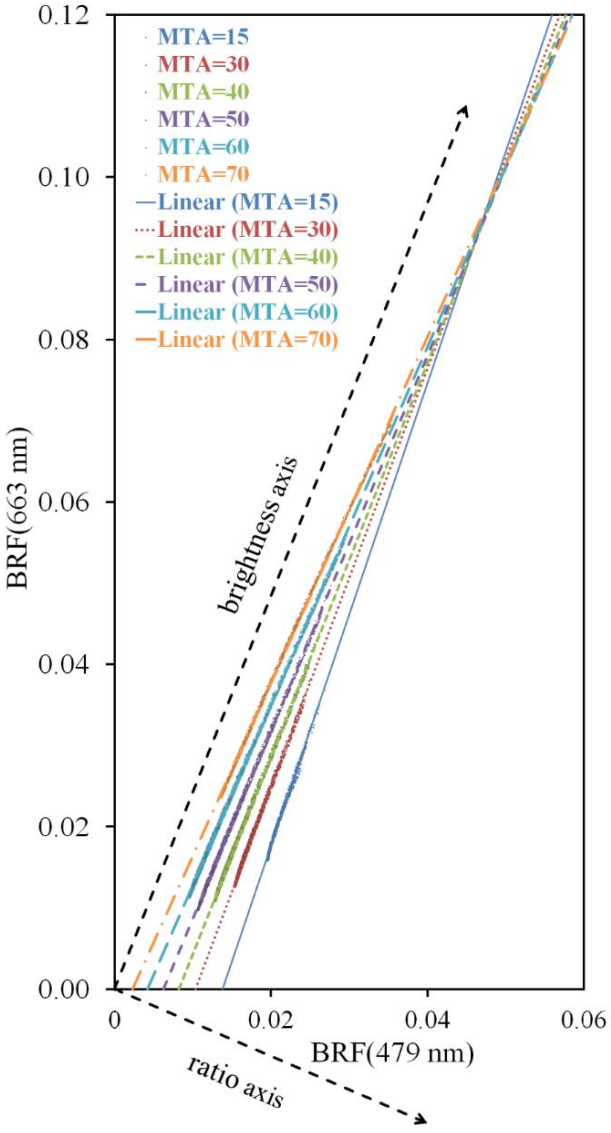

Fig. 16. Reflectance in blue (479 nm) and red (663 nm) for different MTA values (MTA=15º, 30º, 40º, 50º, 60º and 70º) according to PROSAIL simulations. The rotated axes were defined as "brightness axis" and "ratio axis". The ratio axis was used for retrieving MTA.

MTA curves. The RDs of slope and intercept for REIP were small; the values were both approximately 0.1 (III Fig. 7). Two of the VIs, TCARI/OSAVI and CTR6 had the RDs of slope and intercept within 1. In model-simulated and empirical data, these three indices, REIP, TCARI/OSAVI and CTR6 had a relatively high correlation (model: $R^2 > 0.62$ and empirical: $R^2 > 0.40$) with Cab (Fig. 19).

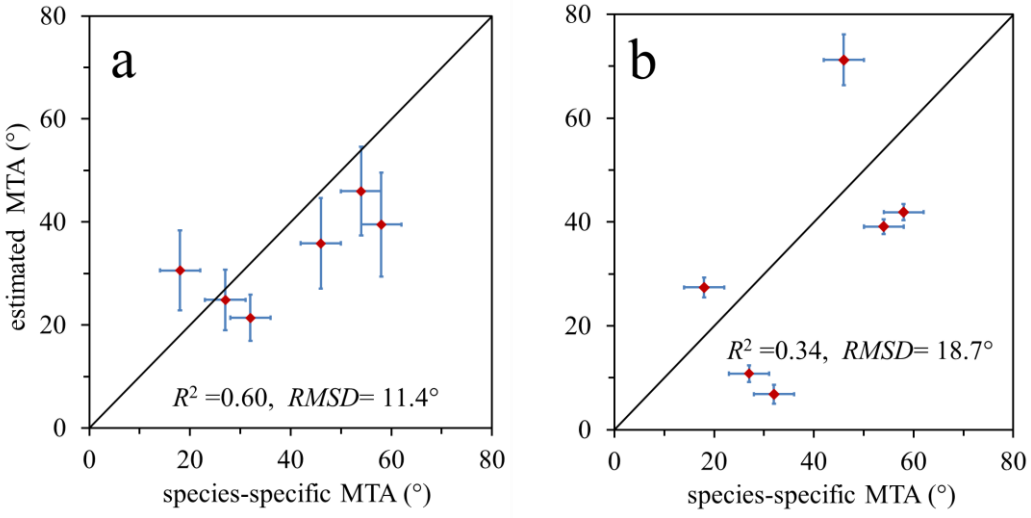

Fig. 17. Comparison of MTA retrieval accuracy for the two methods: a) MTA retrieved using LUT and canopy reflectance at 748 nm vs. field-measured MTA, b) MTA retrieved from reflectance in blue and red vs. field-measured MTA.

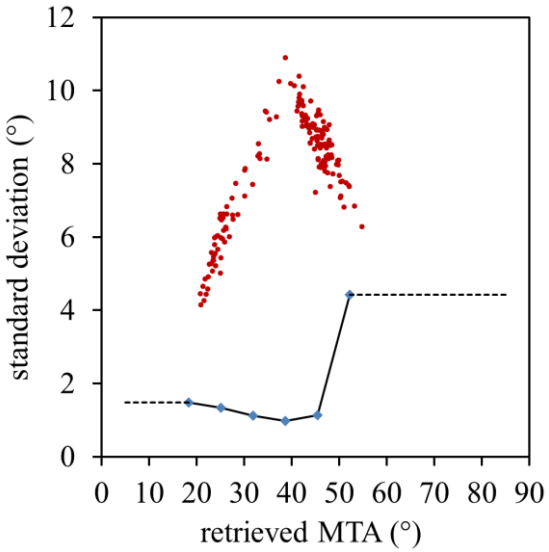

Fig. 18. MTA retrieval uncertainty of the red edge method (red points), and the red-blue method (blue square). For the red edge method, standard deviation values were calculated for each retrieved MTA. For the red-blue method and the MTA values outside 18° – 52° interval, the standard deviation was assumed constant.

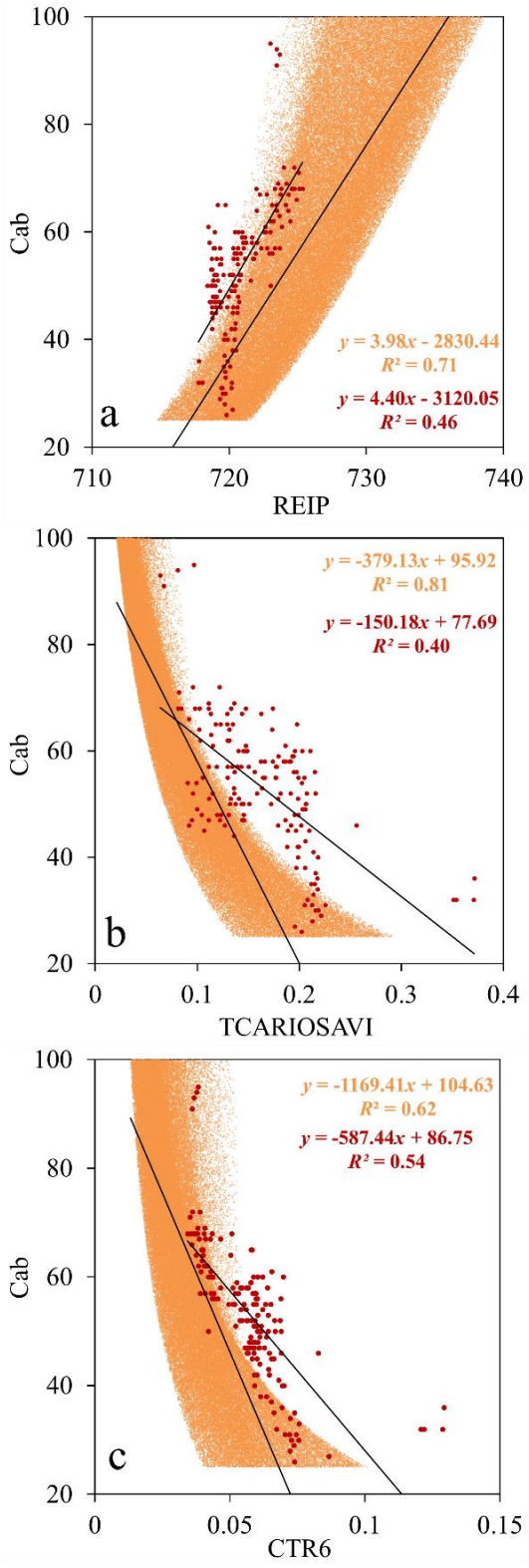

Fig. 19. Correlation between Cab and the three best performing vegetation indices (REIP, TCARI/OSAVI and CTR6) in model-simulated (smaller dense points) and empirical dataset (larger points).

4 DISCUSSION

LAD controls the light interception in the canopy and affects energy and mass balance in the soil-vegetation system. LAD is also a confounding factor for estimating LAI and Cab using optical approaches. An accurate estimation of LAD in both the stand and regional scales is indispensable for understanding radiation and transmission within the vegetation canopy, and contributes to the accurate estimation of parameters of interest, e.g. LAI and Cab. Nevertheless, there is so far no efficient, repeatable and inexpensive method for in situ crop LAD measurement. Moreover, there is no effective remote sensing method for LAD measurement on a large scale. Well-known limitations of traditional LAD measurement methods are that they are laborious, time-consuming and constrained to stand scale. Therefore, new methods are needed to improve the efficiency and accuracy of LAD estimation. Moreover, new methods are required to make it possible for estimating LAD over a large area. This thesis focused on developing new methods for crop LAD measurements. To achieve this goal, two studies were carried out. First of all, this thesis solved the problem of in situ crop LAD measurement, especially for cereal crop species, by including leaf shape function. Secondly, new methods were developed for solving the problem of the remote-sensing method of LAD measurement. The LAD measurement technologies developed in this thesis realized efficient, repeatable and inexpensive estimations of LAD, and also a possibility of mapping LAD over a large area. Quantitative estimations of LAD contributed to the understanding of light interception and radiation distribution within the vegetation canopy. When coupling with the canopy reflectance and transmittance models, accurate estimations of LAD can improve the quantification of LAI and leaf biochemical pigments by getting rid of the confounding effect of LAD.

In this study, MTA was considered because species-specific as it tends to vary more between species than within species (Ross, 1981; Campbell, 1990; Campbell and Norman, 1998; Weiss et al., 2004; Houborge et al., 2007). Thus, although the MTA used in the study was measured at the same crop growing stage one year after the spectroscopic measurement, it is feasible to combine the two measurements. The applicability of species-specific MTA is supported by the strong correlation between photographic and LAI-2000 measurements for five of six species (Fig. 12). The species-specific nature is also confirmed from remote sensing measurements. In spectroscopic MTA measurements, the STD of species-specific MTA was all within 5˚ for the red edge method and within 7˚ for the red-blue axes method (II Table 3). In addition, for the red-blue method, the points belonging to different species were separated on the brightness-ratio axes (II Fig. 5).

For photographic LAD measurements, leaf photographs were taken from a few plots for each species. The plots were assumed to be representative of each species. In addition, the photographs were taken from outside the plots. The representability of the selected plots and the effects of plot edge on LAD measurements are unknown.

Leaf chlorophyll content was converted from SPAD readings using an empirical relationship (Markwell et al., 1995; Vohland et al., 2010). The exact relationship between Cab and SPAD readings is specific to each instrument. Unfortunately, no exact calibration was available for each instrument used in this study. Therefore, the Cab values obtained in this study should be treated with care.

However, the calibrated relationships for different instruments are expected to be similar (Markwell et al., 1995). While the absolute scale of Cab measurements may therefore be biased, the values of the obtained Cab relative to each other are correct.

Compared to LAI-2000 MTA measurements, photographic MTA values were systematically lower. The largest difference was obtained for narrow-leafed lupin. LAI-2000 measured the "effective" MTA or LAI that fitted the best angular distribution of transmittance. The "effective" MTA is affected by other canopy structure characteristics and the tilt angle of canopy elements other than leaves. In the LAI-2000 MTA calculation algorithm, the plant canopy is assumed be horizontally homogeneous and the plant leaves uniformly distributed in the azimuth direction. However, in reality, narrow-leaf lupin has palmate compound leaves attached to long petioles and nearly vertical stems. Although the leaflet in the canopy is flat, as confirmed by our photographs, the more vertical petioles and stems affect the output from LAI-2000. Moreover, the vegetation structure (clumping) increases the transmittance (gap fraction) measurement made under a diffuse sky condition. If the gap fraction increases by the same proportion in each LAI-2000 sensor ring, MTA will be overestimated. This is most likely the case for narrow-leafed lupin.

The PROSAIL model simulated a lower reflectance factor compared with AISA measurements, especially at visible wavelengths. This could partly be attributed to the soil spectrum used in PROSAIL. Differences in soil moisture are expected between the time of airborne spectroscopic data acquisition (25 July 2011) and field spectral measurement after harvest (7 October 2011). Another reason could be the assumptions of the model inputs. For example, Cab and Car were connected in the model input and the brown pigments were ignored, whereas, most of the crops had non-green elements in their canopies such as flowers or heads. Thus, the underestimation is equivalent to having brown elements (at least) at the top of the canopy. Unfortunately, the real value of the brown pigment is not available. The differences between modelled and measured spectra inevitably lead to the difference of R^2 of VIs and Cab correlations (III Fig. 4).

Compared with the two remote sensing MTA retrieval methods, using single reflectance at 748 had better performance than the red-blue method. In theory, based on PROSAIL model simulations, both methods are able to retrieve the MTA of a homogeneous canopy to a satisfactory accuracy. In model simulation, MTA has stronger correlation with red-blue rotated coordinates (Fig. 17) than with reflectance at 748 nm (II Fig. 6). The exact reason of the discrepancy in the performance between the two methods in model-simulated data and empirical data is unknown. This also could be attributed to the assumptions of the model inputs. Reflectance at 748 nm is affected by brown pigments (Peñuelas et al., 2004). These were ignored in the model simulations. Furthermore, some of the non-green materials (e.g., cereal crop ears and flowers) were located at the top of canopy which strengthens their effects on reflectance. The canopy elements other than leaflet have different angular distribution than that of the leaves, thus affecting the MTA estimation from remote sensing data.

The difference of R^2 values (correlation between VIs and Car) between model-simulated and empirical data are not only affected by the model assumptions. The difference was attributed to the different distribution of the model simulated input parameters and that of empirical data. The model input parameters were uniformly distributed, whereas the skewedness of the distribution of LAI, MTA and Cab in

empirical data was clear (III Fig. 1). Another reason might be caused by the statistical correlation between field measured crop parameters.

For the model-simulated data, the best performing index was BGI, a ratio index between blue and green wavelengths. However, this index failed in the empirical data. The reason could be the wavelength. The difference between the model-simulated and measured reflectance factor was large at blue and green wavelengths. The reflectance at the blue wavelength was heavily affected by atmospheric scattering and specular scattering from the leaf surface. The failure of the third best performing index for model-simulated data was for the Vogelmann index, which is calculated from the normalised difference of a spectrum close to the red absorption maximum, where the canopy reflectance is relatively low. The noise in the remote sensing measurement is suspected to be the potential reason.

The one-parameter ellipsoidal LAD model can describe most of the measured vegetation LADs. However, the one-parameter ellipsoidal LAD model cannot describe the bimodal distribution such as extremophile and a more complex model, for example the two-parameter beta distribution (Goel and Strebel, 1984) needs to be employed. When the beta distribution LAD model was tested in PROSAIL, the relationship between canopy reflectance characteristics and MTA did not change from the value the ellipsoidal LAD model obtained. In PROSAIL model inputs, MTA is the exclusive parameter used to quantify horizontal homogenous canopy structure orientation. In reality, the crop canopy is not homogenous, and plant materials are grouped and placed regularly (I Fig. 10). The canopy structure effects on its reflectance are complicated, and it is likely that they are not completely explained by MTA. Although neither of the two remote sensing MTA retrieval methods was able to retrieve the exact MTA of crops, both methods provide information on the species-specific canopy structure.

MTA and LAI have a similar influence on the canopy reflectance spectrum, especially in NIR, which confounded the LAI estimation from remote sensing data. Most of the satellite remote sensing data was from single near-nadir observation. The two MTA remote sensing algorithms provide a possibility to uncouple MTA and LAI effects on canopy reflectance for satellite data, for example, with the next generation hyperspectral sensor HyspIRI proposed by NASA to be mounted on a satellite in low earth orbit. After quantifying MTA, LAI estimation from canopy reflectance could be enhanced. MTA is also a confounding factor for the remote sensing of Cab. The two variables both have an influence on visible and red edge wavelengths. For example, when Cab is estimated from canopy reflectance model inversion, quantified MTA could be used as prior knowledge and reduce the ill-posed problem.

5 CONCLUSIONS AND FUTURE STUDIES

In this thesis, two general results were contributed to the scientific community. The first contribution is that an in situ LAD measurement method was developed and validated for field crops. The second contribution is that new methods were developed for remotely estimating the LAD of field crops. These contributions solved the problem of estimating vegetation LAD. After quantifying canopy LAD, this information could be separated from the optical observations of the canopy and used to improve the estimation of LAI or leaf pigment content (e.g., Cab).

The usability of photographic techniques for crop LAD determination was confirmed. For long curved leaves of cereal crops, leaf angle should be measured on the basis of segments and the relative area of each section should be considered. This method can be used to measure crop LAD efficiently, and the results can be reproduced.

A high correlation between MTA and far red edge reflectance (748 nm) was confirmed for both the PROSAIL model-simulated and empirical data. In the PROSAIL model-simulated data, blue (479 nm) and red (663 nm) reflectance values exhibited dependence on MTA. In the empirical data, the blue and red reflectance values could be used to separate six crop species (assuming species-specific MTA). These two LAD estimation methods can be used for satellite imaging spectroscopy data to produce canopy structure products in the future.

Among the analysed 58 narrow-band vegetation indices, many of them depended on LAI or MTA. Only two indices (TCARI/OSAVI and CTR6) produced strong and similar correlations with Cab in both model-simulated and empirical data, and they were less dependent on LAI and MTA. These two indices can be used to estimate Cab across various canopy structures and species.

The LAD estimation technologies developed in this thesis facilitate the development of remote sensing of vegetation traits using airborne imaging spectroscopy data. However, there is no limitation for applying these methods using satellite imaging spectroscopy data. The results of this thesis enriched the application of imaging spectroscopy data on vegetation and can help to form the foundation of the global mapping of vegetation LAD. Furthermore, they could potentially be used for separating plant species using remote sensing data.

REFERENCES

Anderson, M.C., 1971. Radiation and crop structure. In: Sestak Z., Catsky J. and Jarvis P.G. (eds). Plant Photosynthetic Production Manual of Methods. The Hague, The Netherland: Junk. 77–90.

Anderson, J.M., 1986. Photoregulation of the composition, function, and structure of thylakoid membranes. Annu. Rev. Plant Physiol. 37, 93–136.

Atzberger, C., 2004. Object-based retrieval of biophysical canopy variables using artificial neural nets and radiative transfer models. Remote Sens. Environ. 93, 53-67.

Bacour, C., Baret, F., Beal, D., Weiss, M., Pavageau, K., 2006. Neural network estimation of LAI, fAPAR, fCover and LAI× C ab, from top of canopy MERIS reflectance data: Principles and validation. Remote Sens. Environ. 105, 313-325.

Baldocchi, D.D., Wilson, K.B., Gu, L., 2002. How the environment, canopy structure and canopy physiological functioning influence carbon, water and energy fluxes of a temperate broad-leaved deciduous forest-an assessment with the biophysical model CANOAK. Tree Physiol. 22, 1065–1077.

Banskota, A., Serbin, S. P., Wynne, R. H., Thomas, V., Falkowski, M. J., Kayastha, N., Townsend, P., 2015. An LUT-Based inversion of DART model to estimate forest LAI from hyperspectral data. IEEE J. Sel. Top. Appl. Earth Obs. Remote Sens. 99, 1-14.

Baret, F., Hagolle, O., Geiger, B., Bicheron, P., Miras, B., Huc, M., ... & Leroy, M., 2007. LAI, fAPAR and fCover CYCLOPES global products derived from VEGETATION: Part 1: Principles of the algorithm. Remote Sens. Environ. 110, 275-286.

Baret, F., Guyot, G., 1991. Potentials and limits of vegetation indices for LAI and APAR assessment. Remote Sens. Environ. 35, 161-173.

Berni, J.A.J., Zarco-Tejada, P.J., Suarez, L., Fereres, E., 2009. Thermal and narrowband multispectral remote sensing for vegetation monitoring from an unmanned aerial vehicle. IEEE Trans. Geosci. Remote Sens. 47, 722–738.

Blackburn, G.A., 2007. Hyperspectral remote sensing of plant pigments. J. Exp. Bot., 58, 855−867.

Boegh, E., Soegaard, H., Broge, N., Hasager, C.B., Jensen, N.O., Schelde, K., Thomsen, A., 2002. Airborne multispectral data for quantifying leaf area index, nitrogen concentration, and photosynthetic efficiency in agriculture, Remote Sens. Environ. 81, 179–193

Bonan, G.B., Levis, S., Sitch, S., Vertenstein, M., Oleson, K.W., 2003. A dynamic global vegetation model for use with climate models: concepts and description of simulated vegetation dynamics. Global Change Biol. 9, 1543–1566.

Botha, E.J., Leblon, B., Zebarth, Z., Watmough, E., 2007. Non-destructive estimationof potato leaf chlorophyll from canopy hyperspectral reflectance using the inverted PROSAIL model. Int. J. Appl. Earth Obs. Geoinf. 9, 360 – 374.

Broge, N.H., Leblanc, E. 2001. Comparing prediction power and stability of broadband and hyperspectral vegetation indices for estimation of green leaf area index and canopy chlorophyll density. Remote Sens. Environ. 76, 156-172.

Campbell, G.S., 1990. Derivation of an angle density function for canopies with ellipsoidal leaf angle distributions. Agric. For. Meteorol. 49, 173–176.

Campbell, G.S., Norman, J.M., 1998. An Introduction to Environmental Biophysics, 2nd ed. Springer, New York.

Carter, G.A., Ratios of leaf reflectances in narrow wavebands as indicators of plant stress. Int. J. Remote Sens. 1994, 15, 697–703.

Casa, R., Jones, H.G., 2004. Retrieval of crop canopy properties: a comparison between model inversion from hyperspectral data and image classification. Int. J. Remote Sens. 25, 1119–1130.

Chen, J.M., Black, T.A., 1992. Foliage area and architecture of plant canopies from sunfleck size distributions. Agric. For. Meteorol. 60, 249-266.

Chen, J.M., Liu, J., Cihlar, J., Goulden, M.L., 1999. Daily canopy photosynthesis model through temporal and spatial scaling for remote sensing applications. Ecol. Modell. 124, 99–119.

Colombo, R., Bellingeri, D., Fasolini, D., Marino, C.M., 2003. Retrieval of leaf area index in different vegetation types using high resolution satellite data. Remote Sens. Environ. 86, 120–131.

Colombo, R., Meroni, M., Marchesi, A., Busetto, L., Rossini, M., Giardino, C., Panigada, C., 2008. Estimation of leaf and canopy water content in poplar plantations by means of hyperspectral indices and inverse modeling. Remote Sens. Environ. 112, 1820–1834.

Combal, B., Baret, F., Weiss, M., 2002. Improving canopy variables estimation from remote sensing data by exploiting ancillary information. Case study on sugar beet canopies. Agronomie-Sciences des Productions Vegetales et de l'Environnement, 22, 205-216.

Darvishzadeh, R., Atzberger, C., Skidmore, A., Schlerf, M., 2011. Mapping grassland leaf area index with airborne hyperspectral imagery: a comparison study of statistical approaches and inversion of radiative transfer models. ISPRS J. Photogramm. Remote Sens. 66, 894–906.

Darvishzadeh, R., Matkan, A.A., Ahangar, A.D., 2012. Inversion of a radiative transfer model for estimation of rice canopy chlorophyll content using a lookup-table approach. IEEE J. Sel. Top. Appl. Earth Obs. Remote Sens. 5, 1222-1230.

Darvishzadeh, R., Skidmore, A., Schlerf, M., Atzberger, C., 2008. Inversion of a radiative transfer model for estimating vegetation LAI and chlorophyll in a heterogeneous grassland. Remote Sens. Environ. 112, 2592-2604

Datt, B., 1999. Visible/near infrared reflectance and chlorophyll content in Eucalyptus leaves. Int. J. Remote Sens. 20, 2741−2759.

Daughtry, C.S.T., Walthall, C.L., Kim, M.S., de Colstoun, E.B., McMurtrey, J.E., 2000. Estimating corn leaf chlorophyll concentration from leaf and canopy reflectance. Remote Sens. Environ. 74, 229–239.

Dawson, T.P., Curran, P.J., 1998. A new technique for interpolating red edge position. Int. J. Remote Sens. 19, 2133−2139.

Dennett, M.D., Ishag, K.H.M., 1998. Use of the expolinear growth model to analyze the growth of faba bean, peas and lentils at three densities: predictive use of the model. Ann. Bot. 82, 507 – 512.

de Wit, C.T., 1965. Photosynthesis of Leaf Canopies. Agricultural Research Report no. 663, Wageningen, Netherlands.

Falster, D.S., Westoby, M., 2003. Leaf size and angle vary widely across species: what consequences for light interception? New Phytol. 158, 509–525.

Fang, H., Liang, S., Kuusk, A., 2003. Retrieving leaf area index using a genetic algorithm with a canopy radiative transfer model. Remote Sens. Environ. 85, 257-270.

Féret, J.-B., François, C., Asner, G.P., Gitelson, A.A., Martin, R.E., Bidel, L.P.R., Ustin, S.L., le Maire, G., Jacquemoud, S., 2008. PROSPECT-4 and 5: Advances in the leaf optical properties model separating photosynthetic pigments. Remote Sens. Environ. 112, 3030 – 3043.

Féret, J.-B., François, C., Gitelson, A., Asner, G.P., Barry, K.M., Panigada, C., Andrew, D.R., Jacquemoud, S., 2011. Optimizing spectral indices and chemometric analysis of leaf chemical properties using radiative transfer modelling. Remote Sens. Environ. 115, 2742–2750.

Filella, I., Serrano, L., Serra, J., Peñuelas, J., 1995. Evaluating wheat nitrogen status with canopy reflectance indices and discriminate analysis. Crop Sci. 35, 1400–1405.

Gitelson, A.A., 2012. Nondestructive estimation of foliar pigment (chlorophylls, carotenoids and anthocyanins) contents: evaluating a semianalytical threeband model. In: Thenkabail, P.S., Lyon, J.G., Huete, A. (Eds.), Hyperspectral Remote Sensing of Vegetation. CRC Press, Boca Raton, FL, 141–165.

Gitelson, A.A., Kaufman, Y.J., Stark, R., Rundquist, D., 2002. Novel algorithms for remote estimation of vegetation fraction. Remote Sens. Environ. 80, 76-87.

Gitelson A.A., Merzlyak, M.N., 1994. Quantitative estimation of chlorophyll-a using reflectance spectra: experiments with autumn chestnut and maple leaves. J. Photochem. Photobiol. B. 22, 247–252.

Gitelson, A.A., Merzlyak, M.N., 1997. Remote estimation of chlorophyll content in higher plant leaves. Int. J. Remote Sens. 18, 2691–2697.

Gitelson, A.A., Peng, Y., Masek, J.G., Rundquist, D.C., Verma, S., Suyker, A., Meyers, T., 2012. Remote estimation of crop gross primary production with Landsat data. Remote Sens. Environ. 121, 404-414.

Gitelson, A.A., Vina, A., Ciganda, V., Rundquist, D.C., Arkebauer, T.J., 2005. Remote estimation of canopy chlorophyll content in crops. Geophys. Res. Lett. 32, L08403.

Gobron, N., Pinty, B., Verstraete, M.M., Govaerts, Y., 1997. A semidiscrete model for the scattering of light by vegetation. J. Geophys. Res. D: Atmos. 102, 9431-9446.

Goel, N.S. 1988. Models of vegetation canopy reflectance and their use in estimation of biophysical parameters from reflectance data. Remote Sens. Reviews, 4, 1-212.

Goel, N.S., Rozehnal, I., Thompson, R.L., 1991. A computer graphics based model for scattering from objects of arbitrary shapes in the optical region. Remote Sens. Environ. 36, 73–104.

Goel, N.S., Strebel, D.E., 1983. Inversion of vegetation canopy reflectance models for estimating agronomic variables. I. Problem definition and initial results using the Suits model. Remote Sens. Environ. 13, 487-507.

Goel, N.S., Strebel, D.E, 1984. Simple beta distribution representation of leaf orientation in vegetation canopies. Agron. J. 76, 800–802.

Gong, P., 1999. Inverting a canopy reflectance model using a neural network. Int. J. Remote Sens. 20, 111-122.

Gower, S.T., Kucharik, C.J., Norman, J.M., 1999. Direct and indirect estimation of leaf area index, fAPAR, and net primary production of terrestrial ecosystems. Remote Sens. Environ. 70, 29–51.

Guanter, L., et al., 2014. Global and time-resolved monitoring of crop photosyn-thesis with chlorophyll fluorescence. Proc. Natl. Acad. Sci. U. S. A. 111, E1327–E1333.

Haboudane, D., Miller, J.R., Pattey, E., Zarco-Tejada, P.J., Strachan, I.B., 2004. Hyperspectral vegetation indices and novel algorithms for predicting green LAI of crop canopies: Modeling and validation in the context of precision agriculture. Remote Sens. Environ. 90, 337–352.

Haboudane, D., Miller, J.R., Tremblay, N., Zarco-Tejada, P.J., Dextraze, L., 2002. Integrated narrow-band vegetation indices for prediction of crop chlorophyll content for application to precision agriculture. Remote Sens. Environ. 81, 416-426.

Haboudane, D., Tremblay, N., Miller, J.R., Vigneault, P., 2008. Remote estimation of crop chlorophyll content using spectral indices derived from hyperspectral data. IEEE Trans. Geosci. Remote Sens. 46, 423–437.

Hatfield, J.L., Prueger, J.H., 2010. Value of using different vegetative indices to quantify agricultural crop characteristics at different growth stages under varying management practices. Remote Sens. 2, 562-578.

Heiskanen, J., Rautiainen, M., Stenberg, P., Mõttus, M., Vesanto, V.-H., 2013. Sensitivity of narrowband vegetation indices to boreal forest LAI, reflectance seasonality and species composition. ISPRS J. Photogramm. Remote Sens. 78, 1–14.

Hernández-Clemente, R., Navarro-Cerrillo, R.M., Suárez, L., Morales, F., Zarco-Tejada, P.J., 2011. Assessing structural effects on PRI for stress detection in conifer forests. Remote Sens. Environ. 2011, 115, 2360–2375.

Hernández-Clemente, R., Navarro-Cerrillo, R.M., Zarco-Tejada, P.J., 2012. Carotenoid content estimation in a heterogeneous conifer forest using narrow-band indices and PROSPECT+ DART simulations. Remote Sens. Environ. 127, 298-315.

Hikosaka, K., Hirose, T., 1997. Leaf angle as a strategy for light competition: optimal and evolutionarily stable light-extinction coefficient within a leaf canopy. Ecoscience 4, 501–507.

Hosgood, B., Jacquemoud, S., Andreoli, G., Verdebout, J., Pedrini, G., Schmuck, G., 1994. Leaf Optical Properties Experiment 93 (LOPEX93). Ispra (Italy) EuropeanCommission — Joint Research Centre EUR 16,095 EN (http://ies.jrc.ec.europa.eu/data-portals.html).

Hosoi, F., Nakai, Y., Omasa, K., 2009. Estimating the leaf inclination angle distribution of the wheat canopy using a portable scanning lidar. J. Agric. Meteorol. 65, 297 – 302.

Houborg, R., Anderson, M., Daughtry, C., 2009. Utility of an image-based canopyreflectance modeling tool for remote estimation of LAI and leaf chlorophyllcontent at the field scale. Remote Sens. Environ. 113, 259–274.

Houborg, R., Boegh, E., 2008. Mapping leaf chlorophyll and leaf area index using inverse and forward canopy reflectance modeling and SPOT reflectance data. Remote Sens. Environ. 112, 186-202.

Houborg, R., Soegaard, H., Boegh, E., 2007. Combining vegetation index and model inversion methods for the extraction of key vegetation biophysical parameters using Terra and Aqua MODIS reflectance data. Remote Sens. Environ. 106, 39 – 58.

Hunt, E.R., Doraiswamy, P.C., McMurtrey, J.E., Daughtry, C.S.T., Perry, E.M., Akhmedov, B., 2013. A visible band index for remote sensing leaf chlorophyll content at the canopy scale. Int. J. Appl. Earth Obs. Geoinf. 21, 103–112.

Jacquemoud, S., Bacour, C., Poilve, H., Frangi, J.P., 2000. Comparison of four radiative transfer models to simulate plant canopies reflectance: Direct and inverse mode. Remote Sens. Environ. 74, 471-481.

Jacquemoud, S., Baret, F., Andrieu, B., Danson, F.M., Jaggard, K., 1995. Extraction of vegetation biophysical parameters by inversion of the PROSPECT+ SAIL models on sugar beet canopy reflectance data. Application to TM and AVIRIS sensors. Remote Sens. Environ. 52, 163-172.

Jacquemoud, S., Verhoef, W., Baret, F., Bacour, C., Zarco-Tejada, P.J., Asner, G.P., Ustin, S. L., 2009. PROSPECT+ SAIL models: A review of use for vegetation characterization. Remote Sens. Environ. 113, S56-S66.

James, S.A., Bell, D.T., 2000. Leaf orientation, light interception and stomatal conductance of Eucalyptus globulus ssp. globulus leaves. Tree Physiol. 20,815–823.

Jonckheere, I., Fleck, S., Nackaerts, K., Muys, B., Coppin, P., Weiss, M., Baret, F., 2004. Review of methods for in situ leaf area index determination. Part I. Theories, sensors and hemispherical photography. Agric. Forest Meteorol. 121, 19–35.

Kaasalainen, S., Krooks, A., Liski, J., Raumonen, P., Kaartinen, H., Kaasalainen, M., Puttonen, E., Anttila, K., Mäkipää, R., 2014. Change Detection of Tree Biomass with Terrestrial Laser Scanning and Quantitative Structure Modelling. Remote Sens. 6, 3906–3922.

Knyazikhin,Y., Martonchik, J.V., Diner, D.J., Myneni, R.B., Verstraete, M., Pinty, B., Gobron, N., 1998. Estimation of vegetation leaf area index and fraction of absorbed photosynthetically active radiation from atmosphere-corrected MISR data. J. Geophys. Res. 103, 32239–32256.

Kokaly, R.F., Asner, G.P., Ollinger, S.V., Martin, M.E., Wessman, C.A., 2009. Characterizing canopy biochemistry from imaging spectroscopy and its application to ecosystem studies. Remote Sens. Environ. 113, S78-S91.

Kuusk, A., 1991. The hot-spot effect in plant canopy reflectance, in: Myneni, R.G., Ross, J. (Eds.), Photon-Vegetation Interaction. Springer-Verlag, Berlin Heidelberg, pp. 139 – 159.

Kuusk, A., Nilson, T., 2000. A directional multispectral forest reflectance model. Remote Sens. Environ. 72, 244–252.

Kuusk, A., Nilson, T., Paas, M., Lang, M., Kuusk, J., 2008. Validation of the forest radiative transfer model FRT. Remote Sens. Environ. 112, 51–58.

Lang, A.R.G., 1986. Leaf area and average leaf angle from transmission of direct sunlight. Aust. J. Bot. 34, 349–355.

Lang, A.R.G., Xiang, Y.Q., Norman, J.M., 1985. Crop structure and the penetration of direct sunlight. Agric. For. Meteorol. 35, 83–101.

Lambert, R., Peeters, A., Toussaint B., 1999. LAI evolution of a perennial ryegrass crop estimated from the sum of temperatures in spring time. Agric. For. Meteorol. 97, 1–8.

Lavergne, T., Kaminski, T., Pinty, B., Taberner, M., Gobron, N., Verstraete, M.M., Vossbeck, M., Widlowski, J.-L., Giering, R., 2007. Application to MISR land products of an RPV model inversion package using adjoint and Hessian codes. Remote Sens. Environ. 107, 362−375.

Le Dantec, V., Dufrêne, E., Saugier, B., 2000. Interannual and spatial variation in maximum leaf area index of temperate deciduous stands. For. Ecol. Manage. 134, 71–81.

Le Maire, G., François, C., Dufrêne, E., 2004. Towards universal deciduous broad leaf chlorophyll indices using PROSPECT simulated database and hyperspectral reflectance measurements. Remote Sens. Environ. 89, 1−28.

Le Toan, T., Quegan, S., Davidson, M.W.J., Balzter, H., Paillou, P., Papathanassiou, K., Plummer, S., Rocca, F., Saatchi, S., Shugart, H., Ulander, L., 2011. The BIOMASS mission: Mapping global forest biomass to better understand the terrestrial carbon cycle. Remote Sens. Environ. 115, 2850–2860.

Liang, S., Strahler, A.H., 1993. An analytic BRDF model of canopy radiative transfer and its inversion. IEEE Trans. Geosci. Remote Sens. 31, 1081-1092.

Liu, J., Chen, J., Cihlar, J., Park, W.M., 1997. A process-based boreal ecosystem productivity simulator using remote sensing inputs. Remote Sens. Environ. 62, 158–175.

López-Lozano, R., Casterad, M.A., Herrero, J., 2010. Site-specific management units in a commercial maize plot delineated using very high resolution remote sensing and soil properties mapping. Comput. Electron. Agric. 73, 219–229.

Maccioni, A., Agati, G. Mazzinghi, P., 2001. New vegetation indices for remote measurement of chlorophylls based on leaf directional reflectance spectra. J. Photochem. Photobiol. B. 61, 52–61.

Majasalmi, T., Rautiainen, M., Stenberg, P., Lukeš, P., 2013. An assessment of ground reference methods for estimating LAI of boreal forests. For. Ecol. Manage. 292, 10–18.

Mäkelä, P., Kleemola, J., Jokinen, K., Mantila, J., Pehu, E., Peltonen-Sainio, P., 1997. Growth response of pea and summer turnip rape to foliar application ofglycinebetaine. Acta Agric. Scand. Sect. B Soil Plant Sci. 47, 168–175.

Markwell, J., Osterman, J.C., Mitchell, J., 1995. Calibration of the Minolta SPAD-502 leaf chlorophyll meter. Photosynth. Res. 46, 467 – 472.

Malenovský, Z., Homolová, L., Zurita-Milla, R., Lukeš, P., Kaplan, V., Hanuš, J., Gastellu-Etchegorry, J.P., Schaepman, M.E., 2013. Retrieval of spruce leaf chlorophyll content from airborne image data using continuum removal and radiative transfer. Remote Sens. Environ.131, 85–102.

Mcinerney, D.O., Suarez-Minguez, J., Valbuena, R., Nieuwenhuis, M., 2010. Forest canopy height retrieval using LiDAR data, medium-resolution satellite imagery and kNN estimation in Aberfoyle, Scotland. Forestry, 83, 195–206.

Meroni, M., Colombo, R., Panigada, C., 2004. Inversion of a radiative transfer model with hyperspectral observations for LAI mapping in poplar plantations. Remote Sens. Environ. 92, 195−206.

Moghaddam, M., Dungan, J.L., Acker, S., 2002. Forest variable estimation from fusion of SAR and multispectral optical data. IEEE Trans. Geosci. Remote Sens. 40, 2176–2187.

Morisette, J.T., Baret, F., Privette, J.L., Myneni, R.B., Nickeson, J.E., Garrigues, S., ... Cook, R., 2006. Validation of global moderate-resolution LAI products: A framework proposed within the CEOS land product validation subgroup. IEEE Trans. Geosci. Remote Sens. 44, 1804-1817.

Myneni, R.B., Hoffman, S., Knyazikhin, Y., Privette, J.L., Glassy, J., Tian, Y., Wang, Y., Song, X., Zhang, Y., Smith, G.R., Lotsch, A., Friedl, M., Morisette, J.T., Votava, P., Nemani, R.R., Running, S.W., 2002. Global products of vegetation leaf area and fraction absorbed PAR from year one of MODIS data. Remote Sens. Environ. 83, 214–231.

Neumann, H.H., Den Hartog, G.D., Shaw, R.H., 1989. Leaf-area measurements based on hemispheric photographs and leaf-litter collection in a deciduous forest during autumn leaf-fall. Agric.For. Meteorol. 45, 325–345.

Nevalainen, O., Hakala, T., Suomalainen, J., Mäkipää, R., Peltoniemi, M., Krooks, A., Kaasalainen, S., 2014. Fast and nondestructive method for leaf level chlorophyll estimation using hyperspectral LiDAR. Agric. For. Meteorol. 198, 250–258

Nguy-Robertson, A.L., Peng, Y., Gitelson, A.A., Arkebauer, T.J., Pimstein, A., Herrmann, I., Karnieli, A., Rundquist, D.C., Bonfil, D.J., 2014. Estimating green LAI in four crops: potential of determining optimal spectral bands for a universal algorithm. Agric. For. Meteorol. 192, 140–148.

Nilson T., Kuusk, A., 1989. A reflectance model for the homogenous plant canopy and its inversion. Remote Sens. Environ. 27, 157 – 167.

Norman, J.M., Kustas, W.P., and Humes, K.S., 1995. Source approach for estimating soil and vegetation energy fluxes in observations of directional radiometric surface temperature. Agric. For. Meteorol. 77, 263–293.

Oppelt, N., Mauser, W., 2004. Hyperspectral monitoring of physiological parameters of wheat during a vegetation period using AVIS data. Int. J. Remote Sens. 25, 145– 159.

Peñuelas, J., Filella, I., 1998. Visible and near-infrared reflectance techniques for diagnosing plant physiological status. Trends Plant Sci. 3, 151–156.

Peñuelas J., Munné-Bosch S., Llusià J, Filella I., 2004. Leaf reflectance and photo- and antioxidant protection in field-grown summer-stressed Phillyrea angustifolia. Optical signals of oxidative stress? New Phytol. 162, 115 – 124.

Pinheiro, C., Rodrigues, A.P., de Carvalho, I.S., Chaves, M.M., Ricardo, C.P., 2005.Sugar metabolism in developing lupin seeds is affected by a short-term waterdeficit. J. Exp. Bot. 56, 2705–2712.

Pisek, J., Ryu, Y., Alikas, K., 2011. Estimating leaf inclination and G-function from leveled digital camera photography in broadleaf canopies. Trees. 25, 919–924.

Pisek J., Sonnentag O., Richardson A.D., Mõttus M., 2013. Is the spherical leaf inclination angle distribution a valid assumption for temperate and boreal broadleaf tree species? Agric. For. Meteorol. 169, 186–194.

Praks, J., Kugler, F., Papathanassiou, K.P., Hajnsek, I., Hallikainen, M., 2007. Height estimation of boreal forest: interferometric model-based inversion at L- and X-band versus HUTSCAT profiling scatterometer. IEEE Geosci. Remote Sens. Lett. 4, 466–470.

Rautiainen, M., Stenberg, P., Nilson, T., Kuusk, A., 2004. The effect of crown shapeon the reflectance of coniferous stands. Remote Sens. Environ. 89, 41–52.

Ross, J., Nilson, T., 1965. The extinction of direct radiation in crops, in: Questions on Radiation Regime of Plant Stand. Institute of Physics and Astronomy, Academy of Sciences of Estonian SSR, Tartu, 25–64 (in Russian).

Ross, J., 1981. The radiation regime and architecture of plant stands, in: Lieth, H. (Eds.), Tasks for Vegetation Science, 3, Springer, New York.

Ross J., Marshak, A., 1988. Calculation of canopy bidirectional reflectance using the Monte Carlo method. Remote Sens. Environ. 24, 213–225.

Ryu, Y., Sonnentag, O., Nilson, T., Vargas, R., Kobayashi, H., Wenk, R., Baldocchi, D.D., 2010. How to quantify tree leaf area index in a heterogeneous savanna ecosystem: a multi-instrument and multi-model approach. Agric. Forest Meteorol. 150, 63–76.

Schläpfer D., Borel C.C., Keller J., Itten K.I., 1998: Atmospheric Pre-Corrected Differential Absorption Techniques to Retrieve Columnar Water Vapor. Remote Sens. Environ. 65, 353-366.

Schlerf, M., Atzberger, C., 2006. Inversion of a forest reflectance model to estimate structural canopy variables from hyperspectral remote sensing data. Remote Sens. Environ. 100, 281-294.

Shibayama, M., 2004. Seasonal profiles of polarized reflectance and leaf inclination distribution of wheat canopies. Plant Prod.Sci. 7, 397 – 405.

Sims, D.A., Gamon, J.A., 2002. Relationships between leaf pigment content and spectral reflectance across a wide range of species, leaf structures and developmental stages. Remote Sens. Environ. 81, 337–354.

Sinoquet, H., Thalisawanyangkura, S., Mabrouk, H., Kasemsap, P., 1998. Characterization of the light environment in canopies using 3D digitizing and image processing. Ann. Bot. 82, 203–212.

Smith, N.J., Borstad, G.A., Hill, D.A., Kerr, R.C., 1991. Using high-resolution airborne spectral data to estimate forest leaf area and stand structure. Can. J. For. Res. 21, 1127-1132.

Sone, C., Saito, K., Futakuchi, K., 2009. Comparison of three methods for estimating leaf area index of upland rice cultivars. Crop Sci. 49, 1438–1443.

Soudani, K., François, C., Maire, G.L. Dantec, V.L., Dufrêne, E., 2006. Comparative analysis of IKONOS, SPOT, and ETM+ data for leaf area index estimation in temperate coniferous and deciduous forest stands. Remote Sens. Environ. 102, 161–175.

Steele, M.R., Gitelson, A.A., Rundquist, D.C., 2008. A comparison of two techniques for nondestructive measurement of chlorophyll content in grapevine leaves. Agron. J. 100, 779–782.

Suits, G.H., 1973. The calculation of the directional reflectance of a vegetative canopy. Remote Sens. Environ. 2, 117-125.

Thanisawanyangkura, S., Sinoquet, H., Rivet, P., Cretenet, M., Jallas, E., 1997. Leaf orientation and sunlit leaf area distribution in cotton. Agric. Forest Meteorol. 86, 1–15.

Utsugi, H., 1999. Angle distribution of foliage in individual Chamaecyparis obtusa canopies and effect of angle on diffuse light penetration. Trees 14, 1–9.

Ustin, S.L., Gitelson, A.A., Jacquemoud, S., Schaepman, M., Asner, G.P, Gamon, J. A., Zarco-Tejada, P.J., 2009. Retrieval of foliar information about plant pigment systems from high resolution spectroscopy. Remote Sens. Environ. 113, 67−77

Verhoef, W., 1984. Light scattering by leaf layers with application to canopy reflectance modeling: The SAIL model. Remote Sens. Environ. 16, 125 – 141.

Vermote, E.F., Tanre, D., Deuze, J.L., Herman, M., Morcrette, J.J., 1997. Second simulation of the satellite signal in the solar spectrum, 6S: an overview. IEEE Trans. Geosci. Remote Sens. 35, 675–686.

Verstraete, M.M., Pinty, B., Dickinson, R.E., 1990. A physical model of the bidirectional reflectance of vegetation canopies: 1. Theory. J. Geophys. Res. D: Atmos., 95, 11755-11765.

Vile, D., Garnier, E., Shipley, B., Laurent, G., Navas, M.L., Roumet, C., Lavorel, S., Diaz, S., Hodgson, J.G., Lloret, F., Midgley, G.F., Poorter, H., Rutherford, M.C., Wilson, P.J., Wright, I.J., 2005. Specific leaf area and dry matter content estimate thickness in laminar leaves. Ann. Bot. 96, 1129 – 1136.

Vina, A., Gitelson A.A., Rundquist, D.C., Keydan, G., Leavitt, B., Schepers, J., 2004. Monitoring maize (Zea mays L.) Phenology with remote sensing. Agron. J. 96, 1139–1147.

Vogelman, J.E., Rock, B.N., Moss, D.M., 1993. Red-edge spectral measurements from sugar maple leaves. Int. J. Remote Sens. 14, 1563–1575.

Vohland, M., Mader, S., Dorigo, W., 2010. Applying different inversion techniques to retrieve stand variables of summer barley with PROSPECT + SAIL. Int. J. Appl. Earth Obs. Geoinf. 12, 71 – 80.

Walthall, C.L., Norman, J.M., Welles, J.M., Campbell, G., Blad, B.L., 1985. Simple equation to approximate the bidirectional reflectance from vegetative canopies and bare soil surfaces. Appl. Opt. 24, 383 – 387.

Walthall, C., Dulaney, W., Anderson, M., Norman, J., Fang, H., Liang, S., 2004. A comparison of empirical and neural network approaches for estimating corn and soybean leaf area index from Landsat ETM+ imagery. Remote Sens. Environ. 92, 465-474.

Wang, W.M., Li, Z.L., Su, H.B., 2007. Comparison of leaf angle distribution functions: effects on extinction coefficient and fraction of sunlit foliage. Agric. For. Meteorol. 143, 106–122.

Warren Wilson, J.W., 1967. Stand structure and light penetration. III. Sunlit foliage area. J. Appl. Ecol. 4, 159–165.

Watson, D.J., 1947. Comparative physiological studies on the growth of field crops:I, Variation in net assimilation rate and leaf area between species and varieties, and within and between years. Ann. Bot. 11, 41–76.

Weiss, M., Baret, F., 1999. Evaluation of canopy biophysical variable retrieval performances from the accumulation of large swath satellite data. Remote Sens. Environ. 70, 293-306.

Weiss, M., Baret, F., Garrigues, S., Lacaze, R., 2007. LAI and fAPAR CYCLOPES global products derived from VEGETATION. Part 2: validation and comparison with MODIS collection 4 products. Remote Sens. Environ. 110, 317–331.

Weiss, M., Baret, F., Myneni, R.B., Pragnère, A., Knyazikhin, Y., 2000. Investigation of a model inversion technique to estimate canopy biophysical variables from spectral and directional reflectance data. Agronomie, 20, 3−22.

Weiss, M., Baret, F., Smith, G.J., Jonckheere, I., Coppin, P., 2004. Review of methods for in situ leaf area index (LAI) determination. Part II. Estimation of LAI, errors and sampling. Agric. For. Meteorol. 121, 37–53.

Welles, J.M., Cohen, S., 1996. Canopy structure measurement by gap fraction analysis using commercial instrumentation. J. Exp. Bot. 47, 1335–1342.

Welles, J.M., Norman, J.M., 1991. Instrument for indirect measurement of canopy architecture. Agron. J. 83, 818–825.

Werner, C., Ryel, R.J., Correia, O., Beyschlag, W., 2001. Structural and functional variability within the canopy and its relevance for carbon gain and stress avoidance. Acta Oecol. 22, 129–138.

Wu, C., Niu, Z., Tang, Q., Huang, W., 2008. Estimating chlorophyll content from hyperspectral vegetation indices: Modeling and validation. Agric. For. Meteorol. 148, 1230-1241.

Xie, Q., Huang, W., Liang, D., Chen, P., Wu, C., Yang, G., Zhang, J., Huang, L., Zhang, D., 2014. Leaf area index estimation using vegetation indices derived from airborne hyperspectral images in winter wheat. IEEE J. Sel. Topics Appl. Earth Observ. Remote Sens. 7, 3586–3594.

Zarco-Tejada, P.J., Miller, J.R., Morales, A., Berjón, A., Agüerad, J., 2004. Hyperspectral indices and model simulation for chlorophyll estimation in open-canopy tree crops. Remote Sens. Environ. 90, 463−476.

Zarco-Tejada, P.J., Berjón, A., López-Lozano, R., Miller, J.R., Martín, P., Cachorro, V., De Frutos, A., 2005. Assessing vineyard condition with hyperspectral indices: Leaf and canopy reflectance simulation in a row-structured discontinuous canopy. Remote Sens. Environ. 99, 271-287.

Zhang, Y., Chen, J., Miller, J., Noland, T., 2008. Leaf chlorophyll content retrieval from airborne hyperspectral remote sensing imagery. Remote Sens. Environ. 112, 3234–3247.

Zhu, Y., Wang, W., Yao, X., 2012. Estimating leaf nitrogen concentration (LNC) of cereal crops with hyperspectral data. In: Thenkabail, P.S., Lyon, J.G., Huete, A. (Eds.), Hyperspectral Remote Sensing of Vegetation. CRC Press, Boca Raton, FL, 187–206.